Density Functional Theory Models for Radiation Damage*

S.L. Dudarev

EURATOM/CCFE Fusion Association, Culham Center for Fusion Energy, Oxfordshire OX14 3DB, United Kingdom; email: sergei.dudarev@ccfe.ac.uk

Annu. Rev. Mater. Res. 2013. 43:35–61

The *Annual Review of Materials Research* is online at matsci.annualreviews.org

This article's doi: 10.1146/annurev-matsci-071312-121626

This article is part of the Computational Materials keynote topic compilation.

Keywords

ab initio models, radiation defects, radiation embrittlement, transmutation, helium, vacancies, self-interstitial atoms, clusters, magnetism, defects, dislocations, radiation effects, alloys, collision cascades, energy losses, fusion reactor materials, fission reactor materials, DFT

Abstract

Density functional theory models developed over the past decade provide unique information about the structure of nanoscale defects produced by irradiation and about the nature of short-range interaction between radiation defects, clustering of defects, and their migration pathways. These ab initio models, involving no experimental input parameters, appear to be as quantitatively accurate and informative as the most advanced experimental techniques developed for the observation of radiation damage phenomena. Density functional theory models have effectively created a new paradigm for the scientific investigation and assessment of radiation damage effects, offering new insight into the origin of temperature- and dose-dependent response of materials to irradiation, a problem of pivotal significance for applications.

1. INTRODUCTION

Neutrons and charged particles produced by nuclear reactions in the fuel assembly of a fission power plant (1, 2) or in the deuterium-tritium plasma of a fusion tokamak device (3) induce significant changes in the physical and mechanical properties of materials. These changes result from the interaction of energetic particles with atoms in the materials. For example, neutrons initiate collision cascades, in which radiation defects are formed. These collision cascade events do not change the chemical composition of reactor materials and result only in the formation of fairly stable and relatively well localized distortions of atomic structure; these are the radiation defects. The defects migrate, react, coalesce, and grow. On the mesoscopic (approximately micrometer) scale, the generation of radiation defects gives rise to a particular type of microstructural evolution, which occurs only in irradiated materials. Such changes in microstructure associated with the evolution of defects are termed the accumulation of radiation damage. If the kinetic energy of incident neutrons exceeds a certain threshold value, specific to a particular nuclear reaction, neutron-induced transmutations may also occur. In contrast to collision cascades, transmutation reactions modify the chemical composition of irradiated materials (4). For example, initially chemically pure tungsten bombarded by 14.1-MeV fusion neutrons transmutes into an alloy containing significant amounts of rhenium, osmium, and tantalum. Transmutations also result in the accumulation of helium and other noble gases in the atomic lattice, stimulating swelling and giving rise to helium embrittlement (3).

Understanding the effect of irradiation on materials requires developing atomic-scale models for radiation defects, which describe how the defects evolve and interact. The treatment of reactions between defects in the atomic lattice is broadly similar to the treatment of chemical reactions between molecules. This similarity stems from the fact that defects can be treated as quasi-particles (5) that are characterized by their position, velocity, mass, and effective mobility.

A collision cascade event initiated by a nuclear reaction between an incident neutron (or an ion) and an atomic nucleus results in the displacement of many thousands of atoms from their equilibrium positions (6). Dynamic time-dependent density functional theory (DFT) simulations of collision cascades have so far been limited to events with relatively low impact energy, and the studies themselves have focused almost exclusively on nonmetals (7–12). At the same time, extensive literature describes applications of the (necessarily) simplified models for interatomic forces to the simulation of large-scale, high-energy collision cascade events (13–17). References 18–20 review the experimental observations of defect production by irradiation.

Given that the science of radiation damage phenomena spans over half a century, why have recent DFT (often also referred to as ab initio) studies proved to be so influential? Two aspects of radiation damage elevated the DFT methods to a position of prominence among other scientific means for the investigation of radiation defects. First, defects formed by irradiation are often very small and hence not readily accessible to a direct experimental observation. Second, the simplified models for interatomic forces used for simulating radiation defects before DFT methods became available appeared to be neither sufficiently accurate nor reliable to serve as a starting point for a multiscale treatment of radiation damage phenomena.

In fact, semiempirical interatomic potentials were never meant to provide the starting point for a full quantitative multiscale treatment of radiation damage. For example, the pioneering atomistic simulations of ion channeling effects in Reference 21 were performed by using an interatomic interaction potential that was not assumed to be capable of describing the elastic properties of the crystal. Still, the qualitative insights gained from simulations of radiation damage effects (13–17) had encouraged scientists to apply semiempirical potentials to modeling defects and dislocations, in other words, to cases that were outside the range of validity of interatomic potentials. The result,

as we now know, proved uncertain; for example, the structure of self-interstitial atom (SIA) defects in body-centered-cubic (bcc) metals predicted by using empirical potentials in the 1980s turned out to be incorrect. The predicted core structure of screw dislocations in the same metals also appeared to be incorrect, as did the nature of short-range interaction between vacancies, which turned out to be qualitatively different from what was later found by using electronic structure–based DFT models. These examples are discussed in detail below. At the same time, there are encouraging cases in which focused effort on the development and testing of interatomic potentials has brought remarkable results. Interatomic potentials for iron developed by Mendelev et al. (22), Ackland et al. (23), and Marinica et al. [described in a review article by Malerba et al. (24)] all proved to be sufficiently accurate in describing the structure of dislocation cores and grain boundaries. These potentials also provided a starting point for the development of potentials for the iron-helium binary system (25), in the treatment of which atomistic simulations play an important part, assisting the understanding of the helium grain boundary embrittlement effect. Despite the fact that none of these potentials reproduces the α-γ phase martensitic phase transformation, which determines the properties of iron and iron-based alloys at elevated temperatures, the predicted low-temperature atomic structures agree remarkably well with the structures found in DFT simulations. The embedded atom interatomic potential developed for face-centered-cubic (fcc) copper (26) also proved highly accurate, enabling pioneering simulations of interaction between dislocations and stacking fault tetrahedra (27). Still, given that the characteristic temperature ranges describing the response of a material to irradiation depend very sensitively on the energies of defects derived from simulations, it is essential to employ the most quantitatively accurate methods available as a starting point for the analysis of temperature-dependent manifestations of radiation damage effects. It is very fortunate that DFT provides such a starting point.

We begin by reviewing experimental observations of radiation defects. Determining the structure of radiation defects is difficult not only because these defects are small (19), but also because they randomly move during observation. **Figure 1** illustrates the latter point, showing that if the size of a defect is smaller than ~1 nm, it becomes difficult to unambiguously identify the defect's position in an electron microscope image. This conclusion is supported by a large body of work on in situ electron microscope observation of defects (28–33) and by simulations of electron microscope images (34) that together show that fluctuations of images make it difficult to determine the structure of a defect if its size is in the nanometer size range. Furthermore, in situ observations show that nanoscale radiation defects undergo stochastic thermally activated motion (28, 35), which is further enhanced by the electron beam (36, 37). Other experimental methods, for example, neutron or X-ray diffraction, gather information from fairly large volumes of the material. Interpreting such observations is even more difficult, as the interpretation relies on statistical assumptions about, for example, the orientation of defects, which introduce an extra element of uncertainty into the results.

Atomistic models developed before the publication of the first DFT investigation of radiation defects in iron and Fe-Cu alloys (38) relied on semiempirical parameterizations of interatomic forces (so-called interatomic potentials). An interatomic potential is constructed by using a limited set of parameters characterizing a material, for example, the cohesive energy, elastic constants, and stacking fault energies (39–42). Early attempts to predict the structure of radiation defects using such interatomic potentials—especially the defect structures in which atomic relaxation plays a significant part, such as in the core of a SIA defect—often proved to be incorrect, not only in terms of inaccurately predicted formation and migration energies, but also in terms of incorrectly predicted atomic configurations of defects. DFT calculations have dramatically improved the quality of such predictions, putting simulations of radiation effects on a firm quantitative basis.

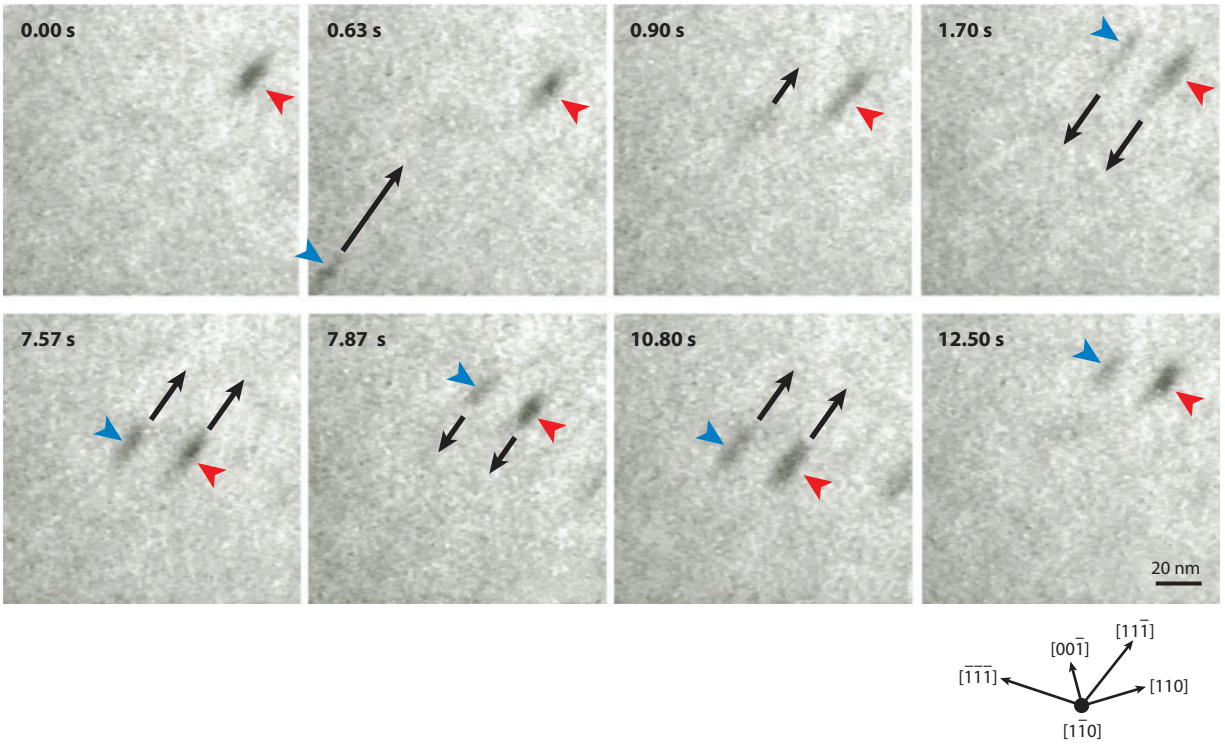

Figure 1

A sequence of in situ electron microscope images showing the dynamics of stochastic motion of two prismatic $\mathbf{b} = a/2[11\bar{1}]$ dislocation loops created in nominally pure iron by ultrahigh-voltage electron irradiation prior to observation. The images show that loops perform one-dimensional random Brownian motion in the direction parallel to their Burgers vector **b** at $T = 673$ K. Arrows indicate the direction of motion of the loops. Observations were performed, by using the $\mathbf{g} = 002$ diffraction condition at 200-kV accelerating voltage, by Arakawa et al. (28).

2. AB INITIO FORMATION AND MIGRATION ENERGIES OF POINT DEFECTS IN ELEMENTAL SOLIDS

Most DFT calculations of defect structures performed so far were carried out by using well-documented DFT computer programs (for a more comprehensive list of the available DFT codes, see **http://www.psi-k.org/codes.shtml**), namely CASTEP (see Reference 43 and **http://www.castep.org/**), VASP (see References 44–46 and **http://www.vasp.at/**), SIESTA (see Reference 47 and **http://icmab.cat/leem/siesta/**), PLATO (see Reference 48 and **http://www-staff.lboro.ac.uk/~masdk/plato.html**), PWSCF (see Reference 49 and **http://www.quantum-espresso.org/**), and ABINIT (see Reference 50 and **http://www.abinit.org/**).

We start by considering the most elementary radiation defects, vacancies, and SIAs. Under irradiation, such defects always form in pairs, termed Frenkel pairs, as a result of a process in which an atom is displaced from a lattice site, coming to rest some distance away from its initial position. In such an event, an initially occupied lattice site becomes a vacancy, and the atom that occupied the site becomes embedded in the lattice far away from its original position, forming a SIA defect. Vacancies can also form thermally, for example, through the migration of atoms to

surfaces or grain boundaries (51). For the treatment of equilibrium thermodynamics of defects, the interested reader is referred to References 52 and 53.

2.1. Vacancies

In a DFT calculation, a vacancy defect is formed by removing an atom from a lattice site in a simulation cell and by relaxing the resulting atomic structure. The formation energy of a vacancy is calculated by using the equation

$$E_f(\text{vacancy}) = E_{N-1}(\text{relaxed}) - \left(\frac{N-1}{N}\right) E_N(\text{perfect}),$$

where E_{N-1}(relaxed) is the total energy of the simulation cell with one atom removed and E_N(perfect) is the energy of an N-atom cell with no defects. Indexes $N-1$ and N refer to the total number of atoms in the cell. This equation shows that two separate DFT calculations are required to find the vacancy formation energy. To find a reasonably accurate value of the vacancy formation energy, a relatively modest cell containing fewer than 100 atoms is required.

In bcc metals, relaxation of atomic positions around a vacancy reduces its formation energy by a large fraction of an electron volt in comparison with the energy computed by assuming no atomic relaxation (54, 55). In silicon, atomic relaxation reduces the vacancy formation energy by approximately 1.2 eV, from the unrelaxed value of 4.36 eV to the value of 3.17 eV computed by fully relaxing the positions of atoms surrounding the vacancy site (56). In hexagonal-close-packed (hcp) and fcc metals, atomic relaxation does not have an appreciable effect on E_f (57, 58), although it does affect the vacancy migration energy E_m. The migration energy corresponds to the top of the energy barrier along a pathway, in the multidimensional space of atomic coordinates, which links atomic configurations corresponding to a vacancy situated at one of the two neighboring lattice sites. A brief but comprehensive review of methods for finding the minimum energy pathways is given in Reference 59. Atomic relaxation reduces the calculated vacancy migration energies in copper and nickel by ~0.4 eV (58, 60). We note that the vacancy formation energy in iron is the lowest among all the bcc transition metals (38). **Table 1** gives vacancy formation and migration energies calculated by using DFT for several pure metals and nonmetals. Some of the calculations for fcc metals were performed only recently (206), and there are still many pure elemental materials for which there is no ab initio information available about the vacancy formation and migration energies.

That DFT calculations are able to predict the properties of vacancies in pure materials is very significant. Materials used in structural applications, and even those tested experimentally under well-controlled conditions, contain small amounts of impurities. Impurity atoms, for example, carbon, form bound complexes with vacancies (61), and the effective formation and migration energies of such complexes may differ significantly from the bare values of E_f and E_m given in **Table 1**. The knowledge of bare vacancy formation and migration energies, and the knowledge of the formation and dissociation energies of vacancy-impurity clusters, which can also be derived from DFT (61), has stimulated the development of pioneering quantitative models for microstructural evolution that explicitly take into account interactions between vacancies and impurities (62, 63).

2.2. Self-Interstitial Atom Defects

A SIA defect forms if an extra atom is inserted into the lattice, and the resulting atomic structure is relaxed. A SIA defect is a localized collective many-atom entity that can be treated as a

Table 1 Formation E_f and migration E_m energies of vacancies computed by using DFT for several elemental metals and nonmetals[a]

	Al	Cu	Au	Ni	Pd	Pt	Pu
E_f	0.580[i]	1.04[d]	0.782[i]	1.37,[e] 1.43,[r] 1.65[r]	1.70[j]	1.18[j]	1.31, 1.36, 1.08[t]
E_m	0.57[m]	0.72[d]	–	1.285,[e] 1.08[r]	–	1.51[j]	–
	V	**Nb**	**Ta**	**Cr**	**Mo**	**W**	**Fe**
E_f	2.51[l]	2.99[l]	3.14[l]	2.64[l]	2.96,[j] 2.96[l]	3.56[l]	2.02,[b] 2.07,[k] 2.15[l]
E_m	0.62[l]	0.91[l]	1.48[l]	0.91[l]	1.28[l]	1.78[l]	0.65,[b] 0.67,[k] 0.64[l]
	C	**Si**	**Ge**	**Be**	**Ti**	**Zr**	**Hf**
E_f	8.2[f]	3.17,[c] 3.29[g]	2.3[h]	0.81,[n] 1.09[o]	1.97,[p] 2.13[q]	2.17,[q] 1.86[s]	2.22[q]
E_m	1.7[f]	0.4[g]	–	0.72B, 0.89NB[o]	0.47B, 0.61NB[p]	0.51B, 0.67NB[q]	0.79B, 0.91NB[q]

[a]All values are given in electron volts. The difference between the energies derived from various literature sources represents the measure of uncertainty in the calculated values. Vacancy formation and migration energies in carbon were computed by assuming graphite structure. B and NB refer to basal and nonbasal vacancy migration pathways, respectively.
[b]Reference 38, [c]Reference 56, [d]Reference 58, [e]GGA values (Reference 60), [f]Reference 64, [g]Reference 65, [h]Reference 66, [i]Reference 67, [j]Reference 68, [k]Reference 69, [l]Reference 70, [m]Reference 71, [n]Reference 72, [o]Reference 73, [p]References 74 and 75, [q]Reference 76, [r]Reference 77 [a higher value of 1.65 eV was quoted in a later publication (78)], [s]Reference 79, [t]Reference 80 (for Reference 80, the values correspond to ferromagnetic, antiferromagnetic, and disordered magnetic moment configurations, respectively).

quasi-particle (5, 81). Calculations predict several local energy minima for a SIA defect, where each minimum corresponds to a different orientation of the defect with respect to the crystal lattice (70). The formation energy of a SIA defect in an elemental system is defined as

$$E_f(\text{self-interstitial}) = E_{N+1}(\text{relaxed}) - \left(\frac{N+1}{N}\right) E_N(\text{perfect}),$$

where E_{N+1}(relaxed) is the total energy of a simulation cell containing an extra atom and E_N(perfect) is the energy of an N-atom cell containing no defect. Depending on the initial position of the atom inserted into the lattice, structural relaxation results in different predicted defect configurations.

A SIA defect always involves large relaxation of its atomic environment. For example, the magnitude of inward relaxation of the first-nearest-neighbor shell of atoms around a vacancy in a bcc transition metal does not exceed ~5% (55). At the same time, the magnitude of elastic strain in the core of a SIA defect in a bcc transition metal often approaches 20% (70, 81). Because the distortion of the lattice around a SIA defect is larger than that around a vacancy, DFT calculations of formation and migration energies of SIA defects require using larger simulation cells. A convergent calculation may require using a cell containing $5 \times 5 \times 5$ or even $6 \times 6 \times 6$ unit cells, which in the case of a bcc lattice correspond to 250 or 432 atoms, respectively (see figure 9 of Reference 82). Although such calculations can now be routinely performed by using parallel computers, ab initio data on defect formation and migration energies are still relatively limited. **Table 2** gives the formation and migration energies computed for various SIA configurations in a number of metals and silicon. For the ab initio data on SIA defect formation energies in zirconium, we refer the reader to Reference 79. Reference 83 gives a remarkably extensive compilation of data on point defects in tungsten.

Calculations show that in all the close-packed crystal structures, the formation energies of SIA defects are significantly higher than the formation energies of vacancies. This difference is

Table 2 Formation energies E_f of various self-interstitial configurations computed by using DFT for several metals and nonmetals[a]

	⟨111⟩	⟨110⟩	⟨100⟩	Tetrahedral	Octahedral	E_m
Fe	4.66,[b] 4.45[c]	3.94,[b] 3.75[c]	5.04,[b] 4.75[c]	4.26[c]	4.94[c]	0.34[c]
V	3.37,[d] 3.14[e]	3.65,[d] 3.48[e]	3.92,[d] 3.57[e]	3.84,[d] 3.69[e]	3.96,[d] 3.62[e]	
Nb	5.25[d]	5.60[d]	5.95[d]	5.76[d]	6.06[d]	
Ta	5.83[d]	6.38[d]	7.00[d]	6.77[d]	7.10[d]	
Cr	5.66[d]	5.68[d]	6.64[d]	6.19[d]	6.72[d]	
Mo	7.42,[d] 7.34[e]	7.58,[d] 7.51[e]	9.00,[d] 8.77[e]	8.40,[d] 8.20[e]	9.07,[d] 8.86[e]	
W	9.55[d]	9.84[d]	11.49[d]	11.05[d]	11.68[d]	
Al	1.959[f]	1.869[f]	1.579[f]	1.790[f]	1.978[f]	0.084[f]
Ni	4.69[g]	4.99[g]	4.07[g]	4.69[g]	4.25[g]	0.14[g]
Si	3.84[h]	3.80 (hexagonal)	3.85 (caged)	4.07[h]	4.8	0.18[h]

[a]Migration energies E_m are given only for the most stable configurations. All values are quoted in electron volt units.
[b]Reference 38, [c]Reference 84, [d]References 70 and 81, [e]Reference 85, [f]Reference 86, [g]Reference 77, and [h]Reference 87 for hexagonal-hexagonal diffusive jumps.

consistent with the significantly larger formation volumes of SIA defects in comparison with the formation volumes of vacancies, confirming that the formation of a SIA defect in a close-packed crystal structure gives rise to a much larger elastic distortion of the lattice in comparison with that of a vacancy (88). Also, the fact that the formation energy of a SIA defect is high is consistent with such defects forming only under irradiation and not thermally [only defects with relatively low formation energies, for example, vacancies, form thermally (51)].

2.3. Defects in Ferromagnetic Iron

DFT calculations (38, 69, 81) show that magnetism has a remarkable effect on the structure of vacancy and SIA defects in iron in comparison with other bcc transition metals (see **Figure 2**). The formation energy of a vacancy in iron is the lowest among the bcc transition metals, and the atomic structure of a SIA defect in iron, the ⟨110⟩ dumbbell, is different from the linear ⟨111⟩ crowdion configuration that a SIA defect adopts in nonmagnetic bcc transition metals (70, 81, 89). The structure of SIA defect clusters in iron is also anomalous: A 2-SIA defect adopts a triangular configuration (90), and larger clusters form unusual compact configurations, the structure of which is related to the structure of the C15 Laves phase (91) (see **Figure 3**). No such unusual defect configuration has been found in nonmagnetic bcc transition metals. Another feature characterizing SIA defects in ferromagnetic bcc iron is collective collinear antiferromagnetic ordering of atomic magnetic moments. Antiferromagnetic ordering is particularly strongly pronounced for the Laves phase–related SIA defect clusters (91). Tight-binding calculations (92, 94) exhibit similar patterns of antiferromagnetic ordering of atomic magnetic moments, suggesting that antiferromagnetism is associated with extended collective magnetically ordered electronic states formed in the highly distorted regions of atomic structure around the SIA defects.

3. CLUSTERING OF DEFECTS

Apart from a few remarkable exceptions described below, in all the metals with close-packed crystal structures, radiation defects form clusters. The driving force for clustering in the case of

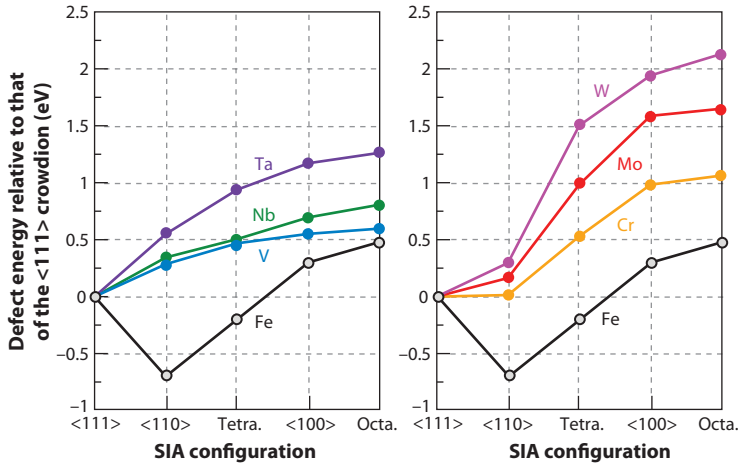

Figure 2

Formation energies of various self-interstitial atom (SIA) defect configurations in body-centered-cubic (bcc) transition metals relative to the formation energy of the ⟨111⟩ crowdion defect configuration (see Reference 81). Note the anomalous pattern of ordering of SIA configurations in ferromagnetic bcc iron. The pattern of ordering of SIA defect energies for each metal correlates well with the metal's position in the periodic table.

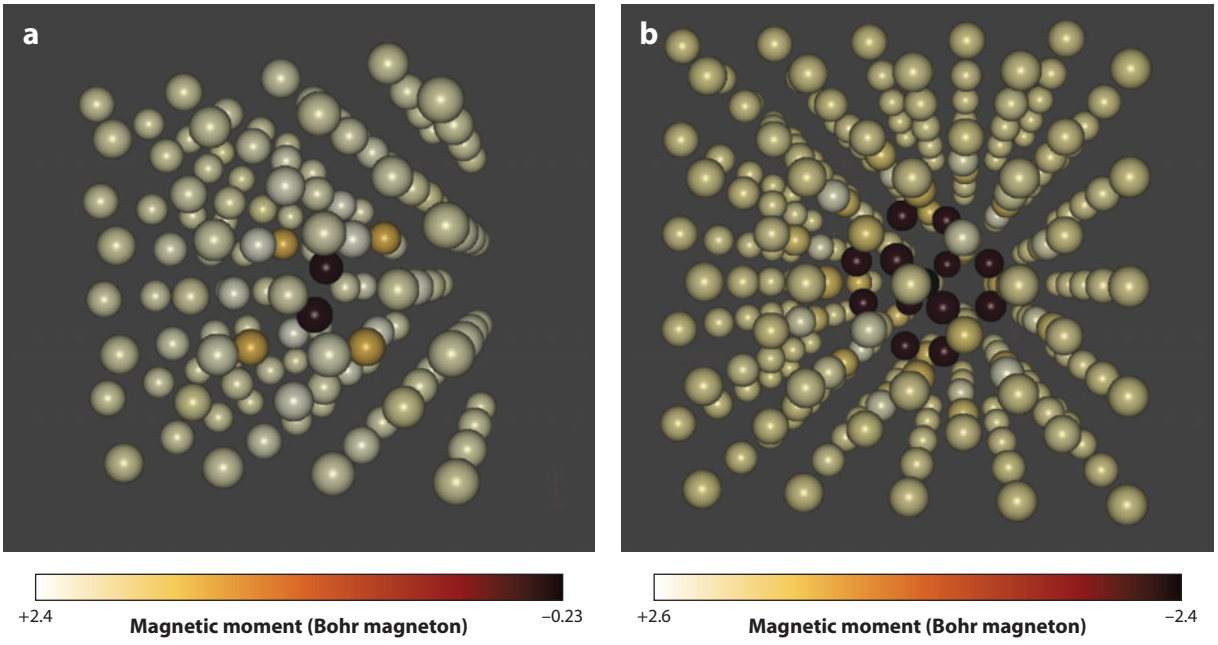

Figure 3

(*a*) Atomic and collinear magnetic structure of a ⟨110⟩ self-interstitial atom defect in iron simulated by using a 128 + 1 atom cell (38, 69, 81). (*b*) Atomic and collinear magnetic structure of a I_2^{C15} two-self-interstitial atom defect computed by using a 250 + 2 atom cell (91). Colors denote the orientation (up or down) and the magnitude of atomic magnetic moments.

SIA defects comes from the large formation energy of an individual SIA defect; this energy results from the large distortion of the lattice around the defects discussed above. This large distortion is partially compensated if defects form clusters, because the energy of an N-defect cluster is lower than the sum of energies of N individual SIA defects. For example, the elastic energy associated with atomic distortion around a 2-SIA cluster is obviously larger than the elastic energy associated with an individual SIA defect. However, due to the extra relaxation occurring in the core of the defect, the 2-SIA elastic energy is still lower than twice the elastic energy associated with a single SIA. This reduction of energy drives the formation of defect clusters. The energy gain occurring if a single SIA defect joins a cluster increases as a function of the cluster size (84, 95). For example, the energy of a 2-SIA defect cluster in bcc α-Fe is $\approx$0.4 eV lower than the sum of energies of two separate SIA defects (84). The energy of a 3-SIA cluster is 1.76 eV lower than the sum of energies of three individual SIA defects and is 1.36 eV lower than the sum of energies of a 2-SIA cluster and a SIA defect. The energy released in the process in which a SIA defect joins a 3-SIA cluster, resulting in the formation of a 4-SIA cluster, is 1.58 eV. The energy of a large defect cluster varies as a function of the number of SIAs, N, in the cluster as $E_N \sim N^\beta$, with, from a purely dimensional argument, $\beta \approx 0.5$ for the case of a planar cluster (a prismatic dislocation loop) (96). For a spherical defect cluster, the value of β is close to 2/3 (83). The energy gain, per SIA defect, associated with the attachment of a SIA defect to a cluster is given by $E_{N+1} - E_N - E_1$. In the limit $N \gg 1$, this quantity asymptotically approaches $(dE_N/dN) - E_1 \approx -E_1$, i.e., minus the formation energy of a SIA defect. Because E_1 is larger in tungsten than in iron, clusters of SIA defects are more stable in tungsten than in iron.

Similarly, the energy gain associated with the attachment of a vacancy to a large vacancy cluster—whether this cluster is a void or a vacancy dislocation loop—is also close to the formation energy of a vacancy. This simple rule does not apply to small vacancy clusters; for example, in many metals, forming a divacancy results in no energy gain. Becquart & Domain (97) found that two vacancies in tungsten repel each other. Somewhat surprisingly, vacancies in tungsten repel each other particularly strongly if they are in the second-nearest-neighbor position. This finding was confirmed by more recent calculations (83, 98) and by a study of divacancies in the entire group of bcc transition metals (89). The latter study pointed out that short-range interaction between vacancies is mediated primarily by electronic structure effects, not by elasticity. The strength and sign of elastic interaction between vacancies (99) are proportional to a linear combination of elastic constants $C_{11} - C_{12} - 2C_{44}$, which is negative for iron and tantalum; is positive for vanadium, niobium, chromium, and molybdenum; and nearly vanishes for tungsten. The strength of the elastic interaction between vacancies does not correlate with the position of a metal in the periodic table, whereas interaction energies predicted by DFT calculations (89) do exhibit such a correlation, confirming that short-range interaction between vacancies is dominated by the electronic structure effects, rather than by elastic effects.

The fact that vacancies in tungsten do not form bound configurations is not a tungsten-specific phenomenon. The same applies to the second-nearest-neighbor divacancies in chromium and molybdenum (89). Also, Carling et al. (100) found that vacancies repel each other in fcc aluminum. Repulsion between vacancies is also found in fcc platinum, gold, and iridium. The attractive interaction between vacancies is exceedingly weak in silver, palladium, nickel, and copper (101). In bcc iron, the divacancy binding energy is 0.2 eV (102). That vacancies in many metals do not form bound complexes lowers the probability of spontaneously nucleating a vacancy cluster. A homogeneous cluster nucleation event occurs only if a certain number of vacancies, ν, spontaneously approach each other and form a bound configuration. The probability of such an event is appreciable only if the critical size of a stable vacancy cluster that can grow further by sequentially attaching individual vacancies from its environment is sufficiently small: $\nu \sim 2$. In aluminum the

critical vacancy cluster size is large—$\nu \approx 8$ (101)—and the probability of nucleating a vacancy cluster is low. This argument illustrates the critical part played by impurity atoms, for example, carbon and helium, that stimulate heterogeneous nucleation of vacancy clusters through the formation of stable vacancy-impurity complexes (83). Alternatively, vacancy clusters may form directly in collision cascades (103, 104). Nucleation of vacancy clusters in collision cascades does not require impurities, and the nucleation rate is proportional to the frequency of cascade events. Clusters of SIA defects also readily form in collision cascades (105).

4. COMPARISON OF DFT CALCULATIONS WITH EXPERIMENTAL OBSERVATIONS

How accurate are the defect formation and migration energies predicted by DFT calculations? Moreover, how useful are the DFT predictions for interpreting experimental information on microstructural evolution of irradiated materials?

To answer these questions, we consider the treatment of resistivity recovery curves in pure iron (106). Resistivity recovery curves describe the gradual recovery of the electrical conductivity of a material that is initially irradiated at a very low temperature and is then relatively slowly heated. Recovery occurs through thermal recombination of radiation defects.

Each type of radiation defect is described by its own characteristic activation energy for migration (for example, DFT predicts that in iron, $E_m \approx 0.34$ eV for a SIA defect and $E_m \approx 0.65$ eV for a vacancy; see **Tables 1** and **2**). We note that all the DFT calculations for bcc iron were performed in the generalized gradient approximation (GGA) because the GGA correctly predicts the bcc ferromagnetic phase to be the ground state of iron, whereas the local-spin-density approximation fails to do so (107).

The conductivity of irradiated samples increases dramatically at certain characteristic temperatures termed resistivity recovery stages. The experimentally observed temperatures of resistivity recovery stages are well documented (108) and can be compared with the corresponding temperatures derived from DFT calculations combined with Monte Carlo modeling of defect migration. Comparing the predicted and experimentally observed temperatures of resistivity recovery stages, Fu et al. (106) found impressive agreement between the migration energies of defects derived from DFT and those observed experimentally. In this way, DFT analysis has made it possible to fully characterize the dynamics of migration and clustering of radiation defects in pure iron.

The determination of the structure of radiation defects is another example in which DFT shows its high predictive capacity. X-ray diffuse scattering experiments performed in the 1970s suggested that a SIA defect in molybdenum adopts a ⟨110⟩ dumbbell configuration (109). DFT calculations (81, 85, 110) showed that the most stable SIA configuration in molybdenum is not a ⟨110⟩ dumbbell but a ⟨111⟩ crowdion. This finding is indicative of a general trend exhibited by SIA defects in all the bcc transition metals (81) (see also **Figure 2**). The DFT prediction that the most stable configuration of a SIA defect in molybdenum is a ⟨111⟩ crowdion also explains the unusually low temperature of resistivity recovery stage I in this metal; this low-temperature stage is related to the onset of thermally activated mobility of crowdions (111). DFT successfully resolves the problem of low-temperature resistivity recovery stages present in all the nonmagnetic bcc transition metals; these stages occur due to the formation of highly mobile ⟨111⟩ SIA configurations. Moreover, DFT calculations show that the determination of the ⟨110⟩ dumbbell SIA defect structure from X-ray diffuse scattering data in Reference 109 is inconsistent with other available experimental and theoretical data and is likely incorrect. In fact, a SIA defect in molybdenum, as well as in all the other nonmagnetic transition bcc metals, adopts a ⟨111⟩ configuration rather than a ⟨110⟩ configuration.

Finally, we note a recent DFT-based study of self-diffusion in aluminum performed by Mantina et al. (71). The problem of self-diffusion is fundamentally related to radiation damage because self-diffusion is mediated by vacancies, which in this case are formed thermally, as opposed to being generated by irradiation. DFT calculations allow one not only to evaluate the formation and migration energies of vacancies, but also to calculate the corresponding entropies and to enable comparison between the 0 K DFT data and the data derived from the high-temperature self-diffusion experiments. The excellent agreement between DFT calculations and experimental observations found in Reference 71 illustrates the strong predictive capabilities of ab initio DFT methods.

5. DFT MODELS FOR DISLOCATIONS

Dislocations are the carriers of plastic deformation of crystalline materials. In bcc transition metals, including ferritic-martensitic and ferritic steels, thermally activated mobility of screw dislocations with a Burgers vector $\mathbf{b} = (a/2)\langle 111\rangle$ controls the observed temperature variation of plastic properties (112, 113). Below a certain temperature, termed the brittle-ductile transition temperature, T_{BDT} (this temperature is not a material's property because it depends on the deformation strain rate), a bcc metal subjected to deformation undergoes brittle fracture. If the temperature of the material is higher than T_{BDT}, the mode of deformation is ductile. Experimental observations (114–116) show that fracture of a bcc metal is a thermally activated process and is characterized by a well-defined activation energy E_{BDT} that—as opposed to T_{BDT}—is independent of the deformation strain rate. The experimentally observed value of E_{BDT} for a single crystal is approximately one-half of the formation energy of a double kink on a $\mathbf{b} = a/2\langle 111\rangle$ screw dislocation (117). Ventelon and colleagues (118, 119) combined DFT and semiempirical potentials calculations and computed the formation energy of a double kink on a $\mathbf{b} = a/2\langle 111\rangle$ screw dislocation in bcc iron $E_{\mathrm{dk}}(\mathrm{Fe}) = 0.65$ eV (119). This value agrees well with the experimentally observed activation energy for the brittle-ductile transition, $E_{\mathrm{BDT}} \approx E_{\mathrm{dk}}/2 = 0.33$ eV (114–116). Applying the same rule, which states that the activation energy for the brittle-ductile transition in a single-crystalline bcc metal is close to one-half of the formation energy of a double kink, we find that in tungsten, for which $E_{\mathrm{BDT}} = 1.05$ eV (114), the double-kink formation energy is $E_{\mathrm{dk}}(\mathrm{W}) = 2.1$ eV. This value exactly matches the low-stress double-kink formation energy of 2.1 eV observed by Brunner (120). Similarly, from the fracture data we find that the double-kink formation energy in vanadium is $E_{\mathrm{dk}}(\mathrm{V}) = 0.54$ eV. A convergent DFT model for a kinked screw dislocation in vanadium or tungsten has not yet been developed.

Both a method for calculating the double-kink formation energy and a statistical model for the nucleation and diffusion of kinks on screw dislocations (121) are required to solve the problem of radiation embrittlement, the central problem of nuclear materials science. Radiation embrittlement of structural (for example, fission reactor pressure vessel) steels (1, 2) is a phenomenon in which T_{BDT} increases monotonically as a function of irradiation dose (122–124). The necessity for controlling radiation embrittlement is easy to appreciate if one considers how a structural material, performing a certain function in a nuclear engineering system at temperature T, responds to deformation after accumulating a certain irradiation dose ϕ. Once the condition $T = T_{\mathrm{BDT}}(\phi)$ is reached as a result of exposure of the material to irradiation, the material becomes brittle, potentially resulting in the loss of structural integrity of the relevant component.

Another issue associated with the structure of screw dislocations in a bcc metal that DFT has recently helped resolve is the configuration of the dislocation core. Whereas the long-range elastic field of a dislocation is well described by elasticity (125), the structure of the dislocation core is not very well known. Simulations performed in the past by using semiempirical interatomic potentials

predicted that the core of a $\mathbf{b} = (a/2)\langle 111\rangle$ screw dislocation in a bcc metal was degenerate, i.e., that its configuration was similar to the configurations shown in figure 12 of Reference 126 and figure 2 of Reference 127. This has direct implications for dislocation mobility (128); for example, the hypothesis about the degenerate dislocation core structure implies the occurrence of several different types of kinks (129). Thermally activated mobility of a screw dislocation with a degenerate core would then exhibit not one but several different activation energies. In experiments, only a single unique activation energy for fracture is observed (114–116), suggesting that the core structure of a screw dislocation is not degenerate.

This assertion agrees with the findings by Ismail-Beigi & Arias (130) and by Frederiksen & Jacobsen (131), who simulated screw dislocations in various nonmagnetic bcc metals by using DFT and concluded that "the calculations point to symmetric core structures for all the studied metals." Subsequent work (118, 119, 132) showed that the core structure of screw dislocations in ferromagnetic bcc iron is also nondegenerate. Quantum-mechanical tight-binding models (133–135), parameterized by using DFT data, also predict nondegenerate dislocation cores.

Gilbert, Dudarev, and colleagues (136, 137) identified the origin of, and resolved, the fundamental disagreement between the core structures of $\mathbf{b} = (a/2)\langle 111\rangle$ screw dislocations predicted by DFT and by semiempirical potentials. To do this, they investigated how the energy of a crystal varies if a $\langle 111\rangle$ atomic row of atoms (such atomic rows, or strings, can be seen in **Figure 4**; please see References 136 and 137 for more detail) is translated, as a rigid object, through the crystal. It turns out that the shape of this energy-string translation curve determines the dislocation core structure. **Figure 4** shows examples of the atomic string energy-displacement curves computed by using DFT for all the bcc transition metals. According to the analysis presented in References 136 and 137, if a $\langle 111\rangle$ string energy-displacement curve derived from a semiempirical potential matches the corresponding DFT curve, the core of a $\mathbf{b} = (a/2)\langle 111\rangle$ screw dislocation is nondegenerate (136, 137). All the semiempirical potentials developed by using the criterion described in References 136 and 137 predict nondegenerate core structures of $\mathbf{b} = (a/2)\langle 111\rangle$ screw dislocations.

Concluding this section, we note that Itakura et al. (138) recently published an illuminating DFT study of screw dislocation mobility in iron. These researchers also found a unique minimum energy pathway for screw dislocation migration, with no change in the core structure. Recent DFT simulations of screw dislocation mobility in nonmagnetic bcc transition metals show that the transition pathways for dislocation migration are broadly similar to those characterizing bcc iron.

6. RADIATION DEFECTS IN ALLOYS

There is an extensive literature on the application of DFT to the analysis of structural stability and phase transformations in alloys (see, e.g., References 139–141). At the same time, relatively little is known about the structure of radiation defects in alloys. Applying DFT to alloys is difficult because an alloy is a complex statistical object for which a certain chemical composition can be realized with many possible atomic configurations. The structure of a defect then depends on the choice of both the alloy atomic configuration and the defect site. **Figure 5** shows how strongly the formation energy of a vacancy fluctuates as a function of its lattice site in bcc W-Ta alloys (98). **Figure 5** also shows that the formation energy of a defect in an alloy is a relatively ill-defined quantity because this energy is sensitive to the local atomic environment. Strongly fluctuating defect formation and migration energies represent the defining feature of an alloy as opposed to a pure material.

In the context of DFT studies of radiation defects, Fe-Cr binary alloys have attracted the greatest attention because (*a*) iron and chromium are the main constituting elements of ferritic steels

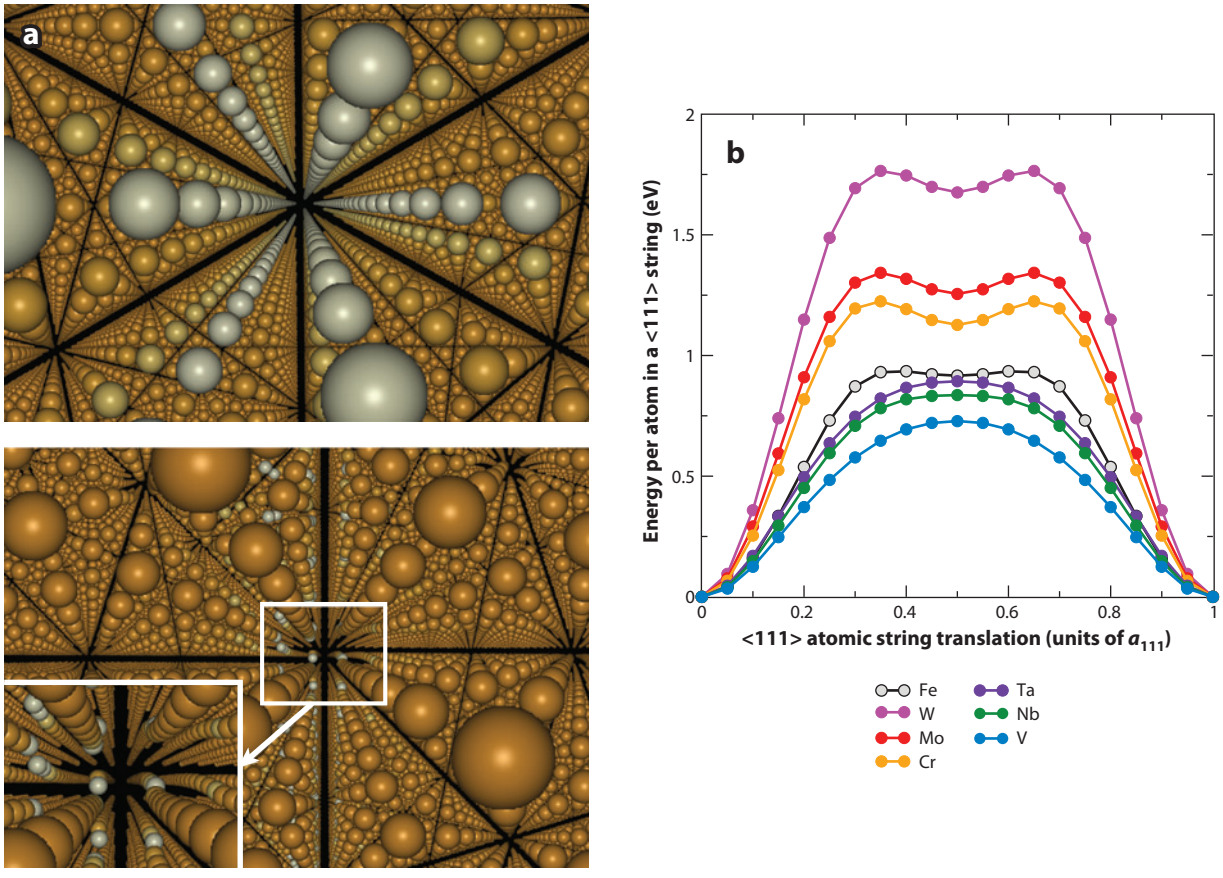

Figure 4

(*a*) The atomic structure of a $\mathbf{b} = (a/2)\langle 111\rangle$ screw dislocation. Such dislocation can be created by rigidly displacing the $\langle 111\rangle$ strings of atoms in the direction parallel to the axes of the strings (see References 136 and 137). (*b*) Density functional theory (DFT) calculations show how the energy of a crystal varies if a $\langle 111\rangle$ string of atoms is displaced through the lattice in the direction parallel to the string itself (111). If the shape of the energy-displacement curve derived from a semiempirical potential matches the corresponding DFT curve shown in this figure, the core of a $\mathbf{b} = (a/2)\langle 111\rangle$ screw dislocation is nondegenerate.

and (*b*) Olsson et al. (142, 143) discovered a magnetic anomaly in the enthalpy of formation of Fe-Cr alloys. DFT calculations show that, in the low-chromium concentration limit, the proximity of chromium atoms does not significantly affect the vacancy formation energy. At the same time, SIA defects interact strongly with chromium atoms (144, 145). Defect migration pathways in Fe-Cr alloys are fairly complex, with activation energies for migration of a SIA defect fluctuating between 0.3 and 0.6 eV (146). In contrast, in pure iron, thermally activated migration of a SIA defect is characterized by a unique activation energy of 0.34 eV (69, 146). A comprehensive investigation of statistical aspects of defect formation and migration in Fe-Cr alloys by Terentyev et al. (147) showed that, in comparison with pure iron, vacancy migration energies fluctuate and vary between 0.2 eV and 1 eV. Strongly fluctuating vacancy migration energies are found not only in Fe-Cr alloys (148) but also in tungsten alloys (see figure 16 of Reference 149). Pareige et al. (150) explored the dynamics of microstructural evolution and phase decomposition of concentrated Fe-Cr alloys, taking into account the effect of a locally fluctuating atomic environment on vacancy migration.

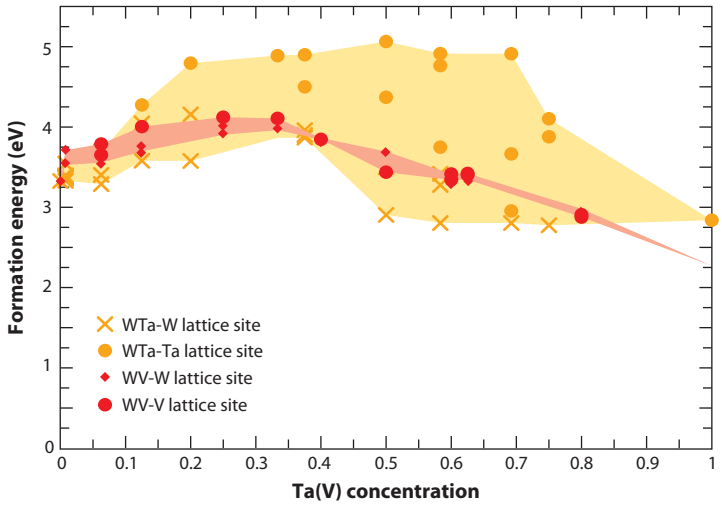

Figure 5

Fluctuating vacancy formation energies computed for the ground-state intermetallic structures of W-Ta and W-V body-centered-cubic binary alloys (see Reference 98).

The magnetic anomaly of the heat of formation of Fe-Cr alloys was discovered by using a simplified model for the alloy, in which fluctuations of the local atomic environment were treated in the mean-field coherent potential approximation (CPA) (142, 143). This approximation is similar to the optical potential approximation used in the statistical theory of scattering (151, 152). CPA was recently also applied to modeling vacancies in ternary Fe-Cr-Ni alloys (153) in the 8–20-at% Ni and 12–24-at% Cr composition range, assuming a paramagnetic fcc crystal structure. The study highlighted the sensitivity of the vacancy formation energy to the chemical composition of the alloy in the vicinity of the (12% Ni, 18% Cr) composition point.

The occurrence of a magnetic anomaly in the heat of formation of Fe-Cr alloys was confirmed by non-CPA DFT calculations (93, 154). Martinez et al. (155) performed an extensive study of vacancy-mediated phase decomposition occurring during aging of Fe-Cr alloys, in which DFT calculations were used for evaluating the transition probabilities of thermally activated vacancy hopping events. Tucker and colleagues (77, 78, 156) used DFT to investigate, for the first time, vacancy-mediated diffusion in ternary Fe-Cr-Ni alloys. Klaver et al. (157) estimated the strength of interaction between radiation defects and the solute atoms in dilute fcc Fe-Cr-Ni alloys, taking constrained (and otherwise unstable) fcc iron as a reference structure. They found that dilute fcc Fe-Cr-Ni alloys exhibit no magnetic anomalies with regard to the properties of defects formed in these alloys. In accord with the earlier work by Tucker et al. (77), Klaver et al. (157) found that chromium was the fastest diffusing element, whereas nickel was the slowest. This finding agrees with experimental information on radiation-induced segregation in steels (158).

By using DFT calculations, it is now possible to perform comprehensive screening of solute elements in terms of their interaction with defects in metals. Olsson et al. (159) and Gorbatov et al. (160) carried out ab initio studies of interaction between (*a*) vacancies and SIAs and (*b*) individual solute atoms in the matrix of ferromagnetic bcc iron and concluded that magnetism has a significant effect on the strength of defect–solute atom interaction. Parameters of vacancy–solute atom interactions derived from ab initio calculations provide input for models describing microstructural evolution of alloys (161, 162).

7. INTERACTION OF RADIATION DEFECTS WITH CARBON, NITROGEN, AND HELIUM

If one takes a naive view of the radiation damage problem, a tempting line of argument would be first to simulate defect formation and migration in pure materials; then to achieve agreement between predictions and experiment; and finally to study more complex cases, including alloys, steels, composite materials, and nanostructural materials. In practice, this is not a viable strategy (163), and it fails for a surprisingly simple reason: Vacancies, SIA defects, and clusters of radiation defects strongly interact with impurities, which are always present in a material. DFT calculations show that impurities form fairly dense atmospheres around radiation defects, especially vacancies, even if the material is nominally pure. The concentration of impurities at a certain distance from a defect is given by the following equation, in atom-per-lattice-site units,

$$c = \frac{c_0 \exp\left(-\frac{U}{k_B T}\right)}{1 + c_0\left[\exp\left(-\frac{U}{k_B T}\right) - 1\right]},$$

where U is the energy of interaction between an impurity and a defect, c_0 is the average concentration of impurities per lattice site in the material far away from the defect, and T is the absolute temperature. For $c_0 = 10^{-6}$, $U = -0.65$ eV [the energy of interaction between a vacancy and a carbon atom in bcc iron (164)], and $T = 500$ K, we find that $c \approx 0.78$. In other words, the concentration of impurities per lattice site in the vicinity of a defect is close to unity. This estimate shows that a vacancy can readily form a bound configuration with a carbon atom, even if the average bulk concentration of carbon atoms in iron is as low as $c_0 = 10^{-6} = 1$ appm.

DFT calculations provide the means for evaluating not only the energy of interaction between radiation defects and impurities, but also various activation energies characterizing reaction rates. Domain and colleagues (61, 165, 166) carried out a pioneering ab initio study of interaction between radiation defects and carbon and nitrogen impurities. Further work by Först et al. (164), Fu et al. (167), and Ohnuma et al. (168) broadly confirmed the findings of Domain et al. (61) and improved the accuracy of predicted binding and activation energies. Calculations show that the most energetically stable configurations of vacancies and carbon atoms in iron are the V-C_2 and V-C_3 complexes (167, 168), whereas the most stable vacancy-nitrogen configuration is V-N_2 (168). DFT calculations performed for tungsten (169, 170) showed that binding between vacancies and impurities in tungsten is stronger than in iron. For example, a V-C complex in tungsten has a binding energy of 1.39 eV (169) [Liu et al. (170) found an even higher value of 1.93 eV], as opposed to a binding energy of 0.65 eV in iron (164, 171). The binding and activation energies calculated by using ab initio methods provide input for kinetic Monte Carlo models (171, 172) that describe the dynamics of evolution of defect-impurity complexes. The accuracy of DFT input is now sufficient to enable meaningful interpretation of experimental data on resistivity recovery in iron (106) and in Fe-Cr alloys (173), including the effect of carbon impurities on vacancy migration (171, 172).

One of the most spectacular findings illustrating the role played by impurities in microstructural evolution of irradiated materials is the discovery of the effect of carbon impurities on helium diffusion and desorption (62, 63, 174, 175). Initially (62), helium desorption curves were interpreted under the assumption that experimental observations could be matched by a microstructural evolution model that took into account reactions between radiation defects and helium in pure iron. Researchers soon discovered that to match observations it was necessary to amend certain critical energy parameters of the model in comparison with DFT data. Further work (63, 174, 175) unambiguously established, by means of more extensive DFT analysis, that to achieve agreement between theoretical predictions and experimental observations it was necessary to take into account the effect of carbon on the reaction rates.

A helium impurity produced by transmutation under neutron irradiation (3, 4) initially occupies an interstitial lattice site and rapidly diffuses through the lattice with an activation energy (in iron and tungsten) of ~0.06 eV (176, 177), eventually forming a helium-vacancy complex (178–181). The binding energy of a helium-vacancy complex is high, varying from 1.2 eV in vanadium to 5 eV in tungsten (181). Alternatively, helium atoms migrating through the lattice may get trapped at a grain boundary, containing vacancy-like sites that are characterized by appreciable local free volume (182). The strength of helium binding to grain boundaries is comparable to the strength of helium binding to vacancies. Magnetism of the host metal is of no significance as far as helium defects are concerned (176, 183), as opposed to the strong effect of magnetism on SIA defects (81) and dislocations (184).

Interstitial helium atoms in tungsten and in iron spontaneously form clusters (177, 180). Clustering occurs because the total energy of a helium cluster is lower than the sum of energies of individual interstitial helium atom defects. In other words, the driving force for clustering of helium atom defects is the same as the driving force for clustering of SIA defects. The formation volume of an interstitial helium atom defect (180, 185) is almost an order of magnitude larger than the formation volume of a SIA defect (38). The formation volume (per helium atom) of a helium cluster is smaller than the formation volume of an individual interstitial helium atom, suggesting that the reduction of elastic energy drives helium clustering.

The fact that the formation volume of a SIA defect is smaller than the formation volume of an interstitial helium atom defect gives rise to an unusual mode of relaxation of large helium atom clusters. Large helium clusters are able to reduce their total energy by spontaneously creating Frenkel pairs, ejecting SIAs and retaining vacancies (180). In contrast, a single substitutional helium defect is unstable with respect to its interaction with a SIA, as the recombination reaction $He_{sub} + SIA \rightarrow He_{int}$ is energetically favorable (180). The optimal ratio of helium atoms to vacancies in a $He_n V_m$ cluster is close to $n/m \approx 1.3$ (180). This estimate also agrees with atomistic simulations of collision cascades (186).

Concluding this section, we note that the average concentration of helium produced by transmutation reactions in the bulk of neutron-irradiated materials is never very high; it does not exceed ~1,000 appm in iron and steels and ~35 appm in tungsten (3, 4). The migration of helium to grain boundaries—where its concentration may reach a critical level, giving rise to grain boundary decohesion (187)—represents a critical stage of the helium embrittlement problem (3).

8. FINITE-TEMPERATURE EFFECTS AND TIME-DEPENDENT AND LARGE-SCALE MODELS

The above discussion shows that it is now possible to compute energies of various defect configurations, including configurations involving several interacting defects, at a high level of accuracy approaching 0.1 eV. Given that large-scale computer facilities are now readily available at almost any university or research laboratory worldwide, performing large-scale DFT calculations has become a relatively routine procedure. To where do these developments shift the focus of research in nuclear fission and fusion materials?

First, most of the DFT computer programs evaluate the energies, and not the free energies, of defect structures. Free energies are required for assessing the thermal stability of defects, and even the stability of alloy phases themselves, at elevated temperatures. The need to extend the DFT methodology to finite temperatures was recently highlighted in the context of application of ab initio models to the development of advanced steels (188). **Figure 6** illustrates this point, showing the contribution of electronic (magnetic fluctuations) and phonon entropies to the free-energy difference between bcc and fcc phases of iron (189). **Figure 6** also shows that, when we

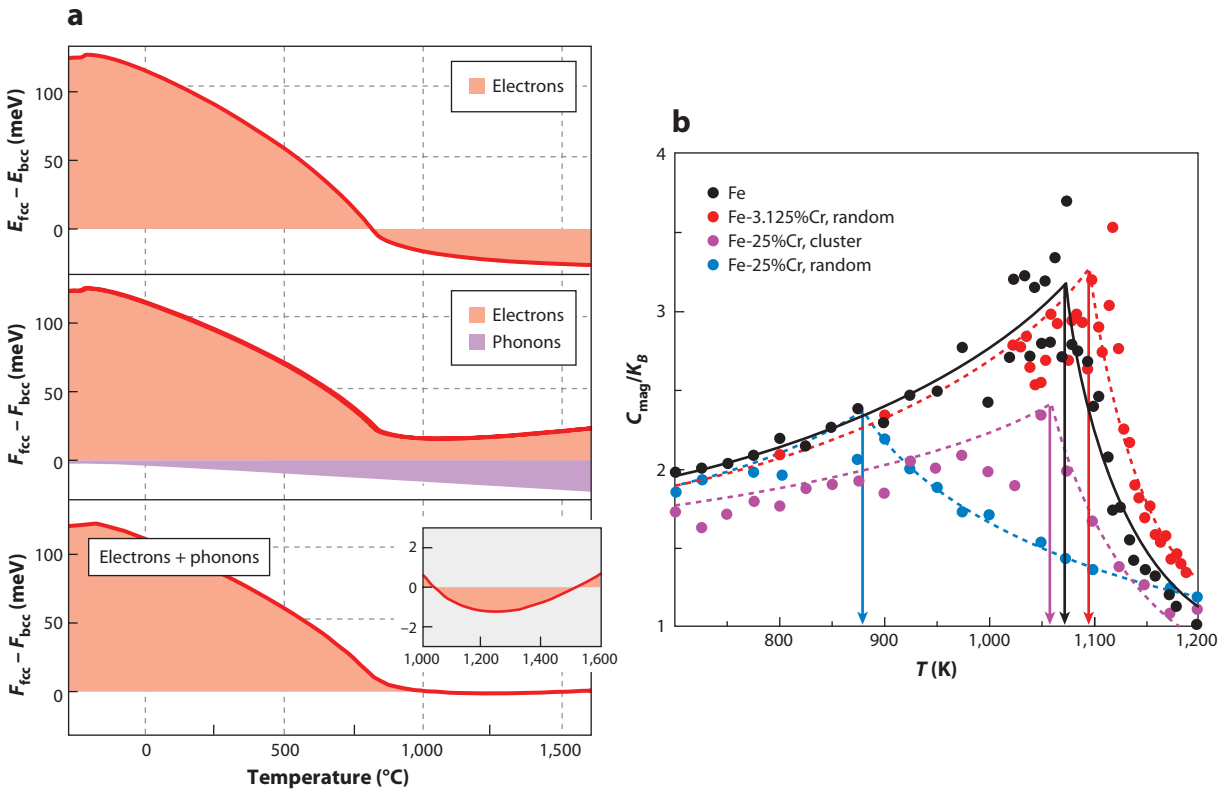

Figure 6

(*a*) (*Top*) The difference between the energies of face-centered-cubic (fcc) and body-centered-cubic (bcc) phases. (*Middle*) The free-energy difference between bcc and fcc phases, shown separately for the electronic (magnetic) and phonon degrees of freedom. (*Bottom*) The total electronic and phonon free-energy difference between fcc and bcc phases. The inset shows a magnified part of the curve exhibiting the α-γ phase transition. The data, in units of meV atom^{-1}, are from Reference 189. (*b*) The Curie temperatures of several Fe-Cr alloys computed by using magnetic cluster expansion. The figure shows that chromium clustering in a Fe-25%Cr alloy results in the Curie temperature of the alloy increasing by more than 150 K (190). Adapted with permission from Lavrentiev et al. (190). Copyright 2011, American Institute of Physics.

compare a random Fe-Cr alloy with an alloy of the same composition containing chromium clusters, the microstructure of an alloy influences its macroscopic magnetic properties, e.g., the Curie temperature, which increases by more than 150 K due to the precipitation and growth of chromium clusters (190).

Second, the size of atomic systems accessible to DFT analysis is in most cases too small. Although in principle one can discuss applications of DFT to systems containing thousands of atoms, in practice most of the calculations are carried out by using supercells containing no more than ~500 atoms. To study atomic configurations involving thousands of atoms, it is necessary to use model Hamiltonians, parameterized by using DFT. For example, the calculations illustrated in **Figure 6** were performed for cells containing many thousands of atoms by using a Heisenberg-Landau Hamiltonian (191, 192) parameterized via the use of DFT data.

Third, DFT calculations are now expected to provide a starting point for the development of large-scale dynamic models, for example, molecular dynamics, in which interatomic interaction

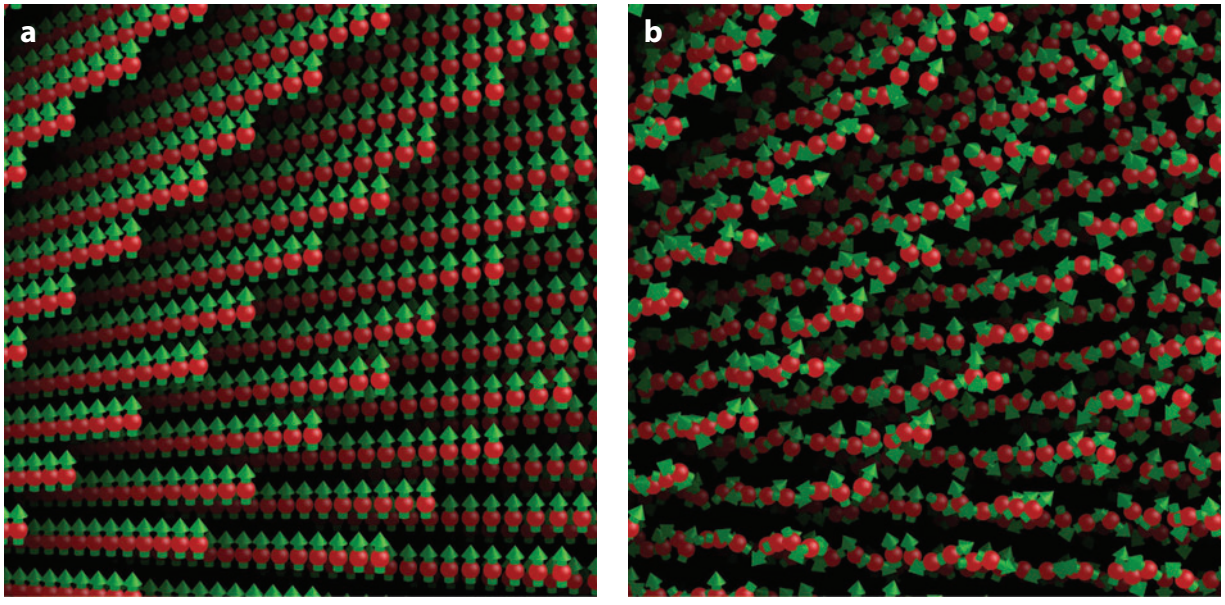

Figure 7

Snapshots illustrating application of spin-lattice dynamics simulations (194, 197) to modeling finite-temperature atomic and magnetic dynamics in iron. (*a*) Body-centered-cubic (bcc) iron at $T = 0$ K, at which magnetic moments are ordered ferromagnetically. (*b*) Bcc iron at $T = 300$ K, at which atoms are randomly displaced from equilibrium lattice positions and magnetic moments fluctuate around the average direction of magnetization. Spin-lattice dynamics simulations were performed by using 54,000 atom cells with periodic boundary conditions (see References 194 and 197).

potentials are fitted to DFT data, often with remarkable success (193). In the case of bcc iron, for which fairly accurate nonmagnetic interatomic potentials for molecular dynamics simulations have been developed, we still face the challenge of developing a dynamic model for the α-γ phase transition. Such a model necessarily requires treating both the dynamics of atoms and atomic magnetic moments (194–197) and hence going beyond conventional molecular dynamics. Spin-lattice dynamics simulations, treating the motion of atoms and evolution of atomic magnetic moments, illustrated in **Figure 7**, should be able to describe the α-γ transition, as well as the changes in the relative stability of defects and dislocations near the transition (184, 198).

Finally, the treatment of the interaction between ions and electrons requires taking into account the fast exchange of energy between ionic and electronic degrees of freedom (199) and—in the case of magnetic metals—between ionic, electronic, and magnetic (200) excitations. This energy exchange is a quantum dissipative process and can be treated by using the notion of dynamic structure factors used in the theory of scattering of fast electrons by crystals (201, 202). Here, DFT calculations should provide the means for evaluating, at a quantitative level of accuracy, the rate of energy losses of fast ions. Whereas it is now possible to derive fairly accurate estimates for the energy loss rate in the limit of high velocity of ions (17), the treatment of energy losses and energy exchange between ions and electrons in the limit of low ion velocity remains an important outstanding issue that has attracted significant attention only recently (203–205).

Ab initio methods have now advanced far enough to enable DFT calculations of free energies; DFT parameterization of large-scale atomistic models, including molecular and spin-lattice dynamics; and the application of DFT to the treatment of energy losses, energy exchange, and relaxation of electronic, magnetic, and atomic degrees of freedom. Addressing such issues will

enable predictive multiscale modeling of radiation damage effects, matching the needs of fission and fusion nuclear materials development and materials engineering.

DISCLOSURE STATEMENT

The author is not aware of any affiliations, memberships, funding, or financial holdings that might be perceived as affecting the objectivity of this review.

ACKNOWLEDGMENTS

The author gratefully acknowledges discussions with I.A. Abrikosov, K. Arakawa, C.S. Becquart, C. Domain, C.-C. Fu, A.P. Horsfield, M.Y. Lavrentiev, P.-W. Ma, M.C. Marinica, D. Mason, D. Nguyen-Manh, G.R. Odette, P. Olsson, S.G. Roberts, A.V. Ruban, A.P. Sutton, F. Willaime, C.H. Woo, and S.J. Zinkle. This work, partly funded by the European Communities under the contract of Association between EURATOM and the Culham Centre for Fusion Energy (CCFE), was carried out within the framework of the European Fusion Development Agreement. The views and opinions expressed herein do not necessarily reflect those of the European Commission. This work was also partly funded by the Research Councils UK (RCUK) Energy Program under grant EP/I501045 under program grant EP/H018921/1 "Materials for Fission and Fusion Power," the EURATOM staff mobility program, and the Engineering and Physical Sciences Research Council (EPSRC) via program grant EP/G050031.

LITERATURE CITED

1. Odette GR, Lucas GE. Embrittlement of nuclear reactor pressure vessels. *J. Miner. Met. Mater. Soc.* 53(7):18–22
2. Odette GR, Nanstad RK. 2009. Predictive reactor pressure vessel steel irradiation embrittlement models: issues and opportunities. *J. Miner. Met. Mater. Soc.* 61(7):17–23
3. Gilbert MR, Dudarev SL, Zheng S, Packer LW, Sublet JC. 2012. An integrated model for materials in a fusion power plant: transmutation, gas production, and helium embrittlement under neutron irradiation. *Nucl. Fusion* 52:083019
4. Gilbert MR, Sublet JC. 2011. Neutron-induced transmutation effects in W and W alloys in a fusion environment. *Nucl. Fusion* 51:043005
5. Dudarev SL. 2003. Coherent motion of interstitial defects in a crystalline material. *Philos. Mag.* 83:3577–97
6. Nordlund K, Ghaly M, Averback RS, Caturla M, Diaz de la Rubia T, Tarus J. 1998. Defect production in collision cascades in elemental semiconductors and fcc metals. *Phys. Rev. B* 57:7556–70
7. Lucas G, Pizzagalli L. 2005. Ab initio molecular dynamics calculations of threshold displacement energies in silicon carbide. *Phys. Rev. B* 72:161202; doi: 10.1103/PhysRevB.72.161202
8. Holmstrom E, Kuronen A, Nordlund K. 2008. Threshold defect production in silicon determined by density functional theory molecular dynamics simulations. *Phys. Rev. B* 78:045202
9. Xiao HY, Gao F, Zu XT, Weber WJ. 2009. Threshold displacement energy in GaN: ab initio molecular dynamics study. *J. Appl. Phys.* 105:123527; doi: 10.1063/1.3153277
10. Xiao HY, Gao F, Weber WJ. 2010. Threshold displacement energies and defect formation energies in $Y_2Ti_2O_7$. *J. Phys. Condens. Mater.* 22:415801; doi: 10.1088/0953-8984/22/41/415801
11. Olsson P, Domain C. 2010. Ab initio study of point defect dynamics: defect clusters and threshold displacement energies in bcc Fe. *Proc. Int. Conf. Multiscale Mater. Model., 5th, Freiburg, Ger., Oct. 4–8*
12. Gao F, Xiao HY, Weber WJ. 2011. Ab initio molecular dynamics simulations of low energy recoil events in ceramics. *Nucl. Instrum. Methods Phys. Res. B* 269:1693–97
13. Seitz F, Koehler JS. 1956. Displacement of atoms during irradiation. In *Solid State Physics*, Vol. 2, ed. F Seitz, D Turnbull, pp. 305–448. New York: Academic

14. Averback RS, Diaz de la Rubia T. 1998. Displacement damage in irradiated metals and semiconductors. In *Solid State Physics*, Vol. 51, ed. H Ehrenreich, F Spaepen, pp. 281–402. New York: Academic
15. Caturla MJ, Marti AG, Jimenez-Rodriguez JJ, Saez JCJ, Perez-Martin MC. 2004. Molecular dynamics simulations of energy deposition in solids. *Adv. Quantum Chem.* 45:79–98
16. Björkas C, Nordlund K. 2007. Comparative study of cascade damage in Fe simulated with recent potentials. *Nucl. Instrum. Methods B* 259:853–60
17. Race CP, Mason DR, Finnis MW, Foulkes WMC, Horsfield AP, Sutton AP. 2010. The treatment of electronic excitations in atomistic models of radiation damage in metals. *Rep. Prog. Phys.* 73:116501
18. Vajda P. 1977. Anisotropy of electron radiation damage in metal crystals. *Rev. Mod. Phys.* 49:481–521
19. Jenkins ML, Kirk MA. 2001. *Characterization of Radiation Damage by Transmission Electron Microscopy*. Bristol, UK: Inst. Phys.
20. Was GS. 2007. *Fundamentals of Radiation Materials Science: Metals and Alloys*. Berlin: Springer. 827 pp.
21. Robinson MT, Oen OS. 1963. Computer studies of the slowing down of energetic atoms in crystals. *Phys. Rev.* 132:2385–98
22. Mendelev MI, Han S, Srolovitz DJ, Ackland GJ, Sun DY, Asta M. 2003. Development of new interatomic potentials appropriate for crystalline and liquid iron. *Philos. Mag.* 83:3977–94
23. Ackland GJ, Mendelev MI, Srolovitz DJ, Han S, Barashev AV. 2004. Development of an interatomic potential for phosphorous impurities in α-iron. *J. Phys. Condens. Matter* 16:S2629–42
24. Malerba L, Ackland GJ, Becquart CS, Bonny G, Domain C, et al. 2010. Ab initio calculations and interatomic potentials for iron and iron alloys: achievements within the Perfect Project. *J. Nucl. Mater.* 406:7–18
25. Gao F, Deng H, Heinisch H, Kurtz RJ. 2011. A new Fe–He interatomic potential based on ab initio calculations in α-Fe. *J. Nucl. Mater.* 418:115–20
26. Mishin Y, Mehl MJ, Papaconstantopoulos DA, Voter AF, Kress JD. 2001. Structural stability and lattice defects in copper: *ab initio*, tight-binding, and embedded-atom calculations. *Phys. Rev. B* 63:224106
27. Marian J, Martinez E, Lee H-J, Wirth BD. 2009. Micro/meso-scale computational study of dislocation-stacking-fault tetrahedron interactions in copper. *J. Mater. Res.* 24:3628–35
28. Arakawa K, Ono K, Isshiki M, Mimura K, Uchikoshi M, Mori H. 2007. Observation of the one-dimensional diffusion of nanometer-sized dislocation loops. *Science* 318:956–59
29. Arakawa K, Arai S, Orihara H, Ono K, Kiritani M. 2002. A study of the mechanism of the growth and shrinkage of stacking fault tetrahedra using the fluctuation of their size under electron irradiation. *J. Electron Microsc.* 51(Suppl. 1):S225–29
30. Arakawa K, Hatanaka M, Mori H, Ono K. 2004. Effects of chromium on the one-dimensional motion of interstitial-type dislocation loops in iron. *J. Nucl. Mater.* 329–333:1194–98
31. Arakawa K, Hatanaka M, Kuramoto E, Ono K, Mori H. 2006. Changes in the Burgers vector of perfect dislocation loops without contact with the external dislocations. *Phys. Rev. Lett.* 96:125506
32. Matsukawa Y, Zinkle SJ. 2007. One-dimensional fast migration of vacancy clusters in metals. *Science* 318:959–62
33. Arakawa K, Amino T, Mori H. 2011. Direct observation of the coalescence process between nanoscale dislocation loops with different Burgers vectors. *Acta Mater.* 59:141–45
34. Zhou Z, Jenkins ML, Dudarev SL, Sutton AP, Kirk MA. 2006. Simulations of weak-beam diffraction contrast images of dislocation loops by the many-beam Howie-Basinski equations. *Philos. Mag.* 86:4851–81
35. Dudarev SL, Gilbert GR, Arakawa K, Mori H, Yao Z, et al. 2010. Langevin model for real-time Brownian dynamics of interacting nanodefects in irradiated metals. *Phys. Rev. B* 81:224107
36. Dudarev SL, Derlet PM, Woo CH. 2007. Driven mobility of self-interstitial defects under electron irradiation. *Nucl. Instrum. Methods Phys. Res. B* 256:253–59
37. Satoh Y, Matsui H, Hamaoka T. 2008. Effects of impurities on one-dimensional migration of interstitial clusters in iron under electron irradiation. *Phys. Rev. B* 77:094135
38. Domain C, Becquart CS. 2001. Ab initio calculations of defects in Fe and dilute Fe-Cu alloys. *Phys. Rev. B* 65:024103
39. Daw MS, Baskes MI. 1983. Semiempirical, quantum mechanical calculation of hydrogen embrittlement in metals. *Phys. Rev. Lett.* 50:1285–88

40. Finnis MW, Sinclair JE. 1984. A simple empirical *N*-body potential for transition metals. *Philos. Mag. A* 50:45–55
41. Daw MS, Baskes MI. 1984. Embedded-atom method: derivation and application to impurities, surfaces, and other defects in metals. *Phys. Rev.* 29:6443–53
42. Foiles SM, Baskes MI, Daw MS. 1986. Embedded-atom-method functions for the fcc metals Cu, Ag, Au, Ni, Pd, Pt, and their alloys. *Phys. Rev. B* 33:7983–91
43. Clark SJ, Segall MD, Pickard CJ, Hasnip PJ, Probert MJ, et al. 2005. First principles methods using CASTEP. *Z. Kristallogr.* 220:567–70
44. Kresse G, Hafner, J. 1994. Ab initio molecular dynamic simulation of the liquid-metal-amorphous semiconductor transition in germanium. *Phys. Rev. B* 49:14251–69
45. Kresse G, Furthmuller J. 1996. Efficient iterative schemes for ab initio total energy calculations using a plane-wave basis set. *Phys. Rev. B* 54:11169–86
46. Kresse G, Joubert D. 1999. From ultra soft pseudopotentials to the projector augmented wave method. *Phys. Rev. B* 59:1758–75
47. Soler JM, Artacho E, Gale JD, García A, Junquera J, et al. 2002. The SIESTA method for ab initio order–N materials simulation. *J. Phys. Condens. Matter* 14:2745–79
48. Kenny SD, Horsfield AP. 2009. PLATO: a localised orbital based density-functional theory code. *Comput. Phys. Commun.* 180:2616–21
49. Giannozzi P, Baroni S, Bonini N, Calandra M, Car R, et al. 2009. QUANTUM ESPRESSO: a modular and open-source software project for quantum simulations of materials. *J. Phys. Condens. Matter* 21:395502
50. Gonze X, Amadond B, Anglade P-M, Beuken J-M, Bottin F, et al. 2009. ABINIT: first-principles approach to material and nanosystem properties. *Comput. Phys. Commun.* 180:2582–615
51. Barnes RS. 1960. The generation of vacancies in metals. *Philos. Mag.* 5:635–46
52. Kraftmakher Y. 2000. *Equilibrium Point Defects and Thermophysical Properties of Metals*. Singapore: World Sci. 328 pp.
53. Murty KL, Charit I. 2013. *An Introduction to Nuclear Materials*. Weinheim, Ger.: Wiley-VCH. 382 pp.
54. Willaime F, Satta A, Nastar M, Le Bacq O. 2000. Electronic structure calculations of vacancy parameters in transition metals: impact on the bcc self-diffusion anomaly. *Int. J. Quantum Chem.* 77:927–39
55. Soderlind P, Yang LH, Moriarty JA, Wills JM. 2000. First-principles formation energies of monovacancies in bcc transition metals. *Phys. Rev. B* 61:2579–86
56. Probert MIJ, Payne MC. 2003. Improving the convergence of defect calculations in supercells: an ab initio study of the neutral silicon vacancy. *Phys. Rev. B* 67:075204
57. Willaime F. 2001. Impact of electronic structure calculations on study of diffusion in metals. *Mater. Sci. Technol.* 17:766–71
58. Andersson DA, Simak SI. 2004. Monovacancy and divacancy formation and migration in copper: a first-principles theory. *Phys. Rev. B* 70:115108; doi: 10.1103/PhysRevB.70.115108
59. Henkelman G, Jóhannesson G, Jónsson H. 2000. Methods for finding saddle points and minimum energy paths. In *Progress in Theoretical Chemistry and Physics*, ed. SD Schwartz, pp. 269–300. Dordrecht, Neth.: Kluwer Acad.
60. Megchiche EH, Pérusin S, Barthelat J-C, Mijoule C. 2006. Density functional calculations of the formation and migration enthalpies of monovacancies in Ni: comparison of local and nonlocal approaches. *Phys. Rev. B* 74:064111; doi: 10.1103/PhysRevB.74.064111
61. Domain C, Becquart CS, Foct J. 2004. Ab initio study of foreign interstitial atom (C, N) interactions with intrinsic point defects in α-Fe. *Phys. Rev. B* 69:144112
62. Ortiz CJ, Caturla MJ, Fu CC, Willaime F. 2007. He diffusion in irradiated α-Fe: an ab initio–based rate theory model. *Phys. Rev. B* 75:100102
63. Ortiz CJ, Caturla MJ, Fu CC, Willaime F. 2009. Influence of carbon on the kinetics of He migration and clustering in α-Fe from first principles. *Phys. Rev. B* 80:134109. Erratum. 2011. *Phys. Rev. B* 83:139905
64. Telling RH, Ewels CP, El-Barbary AA, Heggie MI. 2003. Wigner defects bridge the graphite gap. *Nat. Mater.* 2:333–37
65. El-Mellouhi F, Mousseau N, Ordejón P. 2004. Sampling the diffusion paths of a neutral vacancy in silicon with quantum mechanical calculations. *Phys. Rev. B* 70:205202

66. Spiewak P, Sueoka K, Vanhellemont J, Kurzydlowski KJ, Mlynarczyk K, et al. 2007. Ab initio calculation of the formation energy of charged vacancies in germanium. *Physica B* 401–402:205–9
67. Bottin F, Zéran G. 2007. Formation enthalpies of monovacancies in aluminium and gold under the condition of intense laser irradiation. *Phys. Rev. B* 75:174114; doi: 10.1103/PhysRevB.75.174114
68. Mattsson TR, Mattsson AE. 2002. Calculating the vacancy formation energy in metals: Pt, Pd, and Mo. *Phys. Rev. B* 66:214110
69. Fu CC, Willaime F, Ordejón P. 2004. Stability and mobility of mono- and di-interstitials in α-Fe. *Phys. Rev. Lett.* 92:175503
70. Derlet PM, Nguyen-Manh D, Dudarev SL. 2007. Multiscale modeling of crowdion and vacancy defects in body-centered-cubic transition metals. *Phys. Rev. B* 76:054107
71. Mantina M, Wang Y, Arroyave R, Chen LQ, Liu ZK, Wolverton C. 2008. First-principles calculation of self-diffusion coefficients. *Phys. Rev. Lett.* 100:215901
72. Ganchenkova MG, Borodin VA. 2007. Ab initio study of small vacancy complexes in beryllium. *Phys. Rev. B* 75:054108; doi: 10.1103/PhysRevB.75.054108
73. Middleburgh SC, Grimes RW. 2011. Defects and transport processes in beryllium. *Acta Mater.* 59:7095–103
74. Raji AT, Scandolo S, Mazzarello R, Nsengiyumva S, Harting M, Britton DT. 2009. Ab initio pseudopotential study of vacancies and self-interstitials in hcp titanium. *Philos. Mag.* 89:1629–45
75. Raji AT, Scandolo S, Mazzarello R, Nsengiyumva S, Harting M, Britton DT. 2011. Intrinsic defects and krypton impurity atoms in hcp titanium: a first-principles study. *Phys. Rev. B* 83:054120; doi: 10.1103/PhysRevB.83.054120
76. Vérité G, Willaime F, Fu CC. 2007. Anisotropy of vacancy migration in Ti, Zr and Hf hexagonal close-packed metals from first principles. *Solid State Phenom.* 129:75–81; doi: 10.4028/www.scientific.net/SSP.129.75
77. Tucker JD, Allen TR, Morgan D. 2007. Ab initio defect properties for modelling radiation-induced segregation in Fe-Ni-Cr alloys. *Proc. Int. Symp. Environ. Degradat. Mater. Nucl. Power Syst., 13th, Whistler, B. C., Can., Apr. 19–23*, pp. 1004–14. Red Hook, NY: Curran Assoc.
78. Tucker JD, Najafabadi R, Allen TR, Morgan D. 2010. Ab initio-based diffusion theory and tracer diffusion in Ni-Cr and Ni-Fe alloys. *J. Nucl. Mater.* 405:216–34
79. Domain C, Legris A. 2005. Ab initio atomic-scale determination of point-defect structure in hcp zirconium. *Philos. Mag.* 85:569–75
80. Robert G, Pasturel A, Siberchicot B. 2005. Vacancy formation in δ-plutonium: a density-functional study in the generalized gradient approximation. *Europhys. Lett.* 71:412–17
81. Nguyen-Manh D, Horsfield A, Dudarev SL. 2006. Self-interstitial atom defects in bcc transition metals: group-specific trends. *Phys. Rev. B* 73:020101
82. Cook I, Ward D, Dudarev SL, 2002. Implications of fusion power plant studies for materials requirements. *Plasma Phys. Control. Fusion* 44:B121–36
83. Becquart CS, Domain C, Sarkar U, DeBacker A, Hou M. 2010. Microstructural evolution of irradiated tungsten: ab initio parameterisation of an OKMC model. *J. Nucl. Mater.* 403:75–88
84. Willaime F, Fu CC, Marinica MC, Dalla Torre J. 2005. Stability and mobility of self-interstitials and small interstitial clusters in α-iron: ab initio and empirical potential calculations. *Nucl. Instrum. Methods Phys. Res. B* 228:92–99
85. Han S, Zepeda-Ruiz LA, Ackland GJ, Car R, Srolovitz DJ. 2002. Self-interstitials in V and Mo. *Phys. Rev. B* 66:220101
86. Jesson BJ, Foley M, Madden PA. 1997. Thermal properties of the self-interstitial in aluminum: an ab initio molecular-dynamics study. *Phys. Rev. B* 55:4941–46
87. Leung WK, Needs RJ, Rajagopal G, Itoh S, Ihara S. 1999. Calculations of silicon self-interstitial defects. *Phys. Rev. Lett.* 83:2351–54; doi: 10.1103/PhysRevLett.83.2351
88. Wolfer WG. 2007. The dislocation bias. *J. Comput. Aided Mater. Des.* 14:403–17
89. Ventelon L, Willaime F, Fu C-C, Heran M, Ginoux I. 2012. Ab initio investigation of radiation defects in tungsten: structure of self-interstitials and specificity of di-vacancies compared to other bcc transition metals. *J. Nucl. Mater.* 425:16–21

90. Terentyev DA, Klaver TPC, Olsson P, Marinica MC, Willaime F, et al. 2008. Self-trapped interstitial-type defects in iron. *Phys. Rev. Lett.* 100:145503
91. Marinica M-C, Willaime F, Crocombette J-P. 2012. Irradiation-induced formation of nanocrystallites with C15 Laves phase structure in bcc iron. *Phys. Rev. Lett.* 108:025501
92. Liu G, Nguyen-Manh D, Liu B-G, Pettifor DG. 2005. Magnetic properties of point defects in iron within the tight-binding-bond Stoner model. *Phys. Rev. B* 71:174115
93. Nguyen-Manh D. 2009. Ab-initio modelling of point defect–impurity interaction in tungsten and other bcc transition metals. *Adv. Mater. Res.* 59:253–56
94. Nguyen-Manh D, Dudarev SL. 2009. Model many-body Stoner Hamiltonian for binary FeCr alloys. *Phys. Rev. B* 80:104440
95. Marinica M-C, Willaime F. 2007. Orientation of interstitials in clusters in α-Fe: a comparison between empirical potentials. *Solid State Phenom.* 129:67–74
96. Gilbert MR, Dudarev SL, Derlet PM, Pettifor DG. 2008. Structure and metastability of mesoscopic vacancy and interstitial loop defects in iron and tungsten. *J. Phys. Condens. Matter* 20:345214
97. Becquart CS, Domain C. 2007. Ab initio calculations about intrinsic point defects and He in W. *Nucl. Instrum. Methods Phys. Res. B* 255:23–26
98. Muzyk M, Nguyen-Manh D, Kurzydlowski KJ, Baluc NL, Dudarev SL. 2011. Phase stability, point defects, and elastic properties of W-V and W-Ta alloys. *Phys. Rev. B* 84:104115
99. Hudson TS, Dudarev SL, Caturla MJ, Sutton AP. 2005. Effects of elastic interactions on post-cascade radiation damage evolution in kinetic Monte Carlo simulations. *Philos. Mag.* 85:661–75
100. Carling KM, Wahnström G, Mattsson T, Sandberg N, Grimvall G. 2003. Vacancy concentration in Al from combined first-principles and model potential calculations. *Phys. Rev. B* 67:054101
101. Zhang X, Lu G. 2008. Electronic origin of void formation in fcc metals. *Phys. Rev. B* 77:174102
102. Djurabekova F, Malerba L, Pasianot RC, Olsson P, Nordlund K. 2010. Kinetics versus thermodynamics in materials modelling: the case of the di-vacancy in iron. *Philos. Mag.* 90:2585–95
103. Woo CH, Singh BN. 1992. Production bias due to clustering of point defects in irradiation-induced cascades. *Philos. Mag. A* 65:889–912
104. Woo CH, Singh BN, Semenov AA. 1996. Recent advances in the understanding of damage production and its consequences for void swelling, irradiation creep and growth. *J. Nucl. Mater.* 239:7–23
105. Calder AF, Bacon DJ, Barashev AV, Osetsky YN. 2010. On the origin of large interstitial clusters in displacement cascades. *Philos. Mag.* 90:863–84
106. Fu C-C, Dalla Torre J, Willaime F, Bocquet J-L, Barbu A. 2005. Multiscale modelling of defect kinetics in irradiated iron. *Nat. Mater.* 4:68–74
107. Leung TC, Chan CT, Harmon BN, 1991. Ground state properties of Fe, Co, Ni, and their monoxides: results of the generalized gradient approximation. *Phys. Rev. B* 44:2923–27
108. Takaki S, Fuss J, Kugler H, Dedek U, Schultz H. 1983. The resistivity recovery of high purity and carbon-doped iron following low temperature electron irradiation. *Radiat. Eff.* 79:87–122
109. Ehrhart P. 1978. The configuration of atomic defects as determined from scattering studies. *J. Nucl. Mater.* 69–70:200–14
110. Beeler B, Good B, Rashkeev S, Deo C, Baskes M, Okuniewski M. 2010. First principles calculations for defects in U. *J. Phys. Condens. Matter* 22:505704
111. Fitzgerald SP, Nguyen-Manh D. 2008. Peierls potential for crowdions in the bcc transition metals. *Phys. Rev. Lett.* 101:115504
112. Hirsch PB. 1960. Unpublished presentation given at Int. Crystallogr. Congr., Cambridge, UK
113. Hollang L. 2002. Mechanical properties. In *Purification Process and Characterization of Ultra-High Purity Metals*, ed. Y Waseda, M Isshiki, pp. 305–48. Berlin: Springer
114. Giannattasio A, Tanaka M, Joseph TD, Roberts SG. 2007. An empirical correlation between temperature and activation energy for brittle-to-ductile transitions in single-phase materials. *Phys. Scr.* T128:87–90
115. Tanaka M, Tarleton E, Roberts SG. 2008. The brittle-ductile transition in single-crystal iron. *Acta Mater.* 56:5123–29
116. Tanaka M, Wilkinson AJ, Roberts SG. 2008. Ductile-brittle transition of polycrystalline iron and iron-chromium alloys. *J. Nucl. Mater.* 378:305–11

117. Dudarev SL, Boutard J-L, Lässer R, Caturla MJ, Derlet PM, et al. 2009. The EU programme for modelling radiation effects in fusion reactor materials: an overview of recent advances and future goals. *J. Nucl. Mater.* 386–388:1–7
118. Ventelon L, Willaime F. 2007. Core structure and Peierls potential of screw dislocations in α-Fe from first principles: cluster versus dipole approaches. *J. Comput. Aided Mater. Des.* 14:85–94
119. Ventelon L, Willaime F, Leyronnas P. 2009. Atomistic simulation of single kinks of screw dislocations in α-Fe. *J. Nucl. Mater.* 386–388:26–29
120. Brunner D. 2000. Comparison of flow-stress measurements on high-purity tungsten single crystals with the kink-pair theory. *Mater. Trans. JIM* 41:152–60
121. Swinburne TD, Dudarev SL, Fitzgerald SP, Gilbert MR, Sutton AP. 2013. Theory and simulation of the diffusion of kinks on dislocations in bcc metals. *Phys. Rev. B* 87:064108
122. Steele LE, ed. 1993. *Radiation embrittlement of nuclear reactor pressure vessel steels: an international review*. Spec. Tech. Publ. 1,170, Am. Soc. Test. Mater., Philadelphia. 408 pp.
123. Gaganidze E, Schneider H-C, Dafferner B, Aktaa J. 2007. High-dose neutron irradiation embrittlement of RAFM steels. *J. Nucl. Mater.* 355:83–88
124. van der Schaaf B, Petersen C, De Carlan Y, Rensman JW, Gaganidze E, Averty X. 2009. High dose, up to 80 dpa, mechanical properties of Eurofer-97. *J. Nucl. Mater.* 386–388:236–40
125. Hirth JP, Lothe J. 1982. *Theory of Dislocations*. Malabar, FL: John Wiley & Sons. 2nd ed.
126. Vitek V. 1974. Theory of the core structures of dislocations in body-centred-cubic metals. *Cryst. Lattice Defects* 5:1–34
127. Vitek V. 2004. Core structure of screw dislocations in body-centred cubic metals: relation to symmetry and interatomic bonding. *Philos. Mag.* 84:415–28
128. Cai W, Bulatov VV, Chang JP, Li J, Yip S. 2004. Dislocation core effects on mobility. In *Dislocations in Solids*, ed. FRN Nabarro, JP Hirth, pp. 3–80. Amsterdam: Elsevier
129. Ngan AHW, Wen M. 2001. Dislocation kink-pair energetics and pencil glide in body-centred-cubic crystals. *Phys. Rev. Lett.* 87:075505
130. Ismail-Beigi S, Arias TA. 2000. Ab initio study of screw dislocations in Mo and Ta: a new picture of plasticity in bcc transition metals. *Phys. Rev. Lett.* 84:1499–502
131. Frederiksen SL, Jacobsen KW. 2003. Density functional theory studies of screw dislocation core structures in bcc metals. *Philos. Mag.* 83:365–75
132. Domain C, Monnet G. 2005. Simulation of screw dislocation motion in iron by molecular dynamics simulations. *Phys. Rev. Lett.* 95:215506
133. Mrovec M, Nguyen-Manh D, Pettifor DG, Vitek V. 2004. Bond-order potential for molybdenum: application to dislocation behavior. *Phys. Rev. B* 69:094115
134. Mrovec M, Gröger R, Bailey AG, Nguyen-Manh D, Elsässer C, Vitek V. 2007. Bond-order potential for simulations of extended defects in tungsten. *Phys. Rev. B* 75:104119
135. Mrovec M, Nguyen-Manh D, Elsaässer C, Gumbsch P. 2011. Magnetic bond-order potential for iron. *Phys. Rev. Lett.* 106:246402
136. Gilbert MR, Dudarev SL. 2010. Ab initio multi–string Frenkel-Kontorova model for a $\mathbf{b} = a/2[111]$ screw dislocation in bcc iron. *Philos. Mag.* 90:1035–61
137. Chiesa S, Gilbert MR, Dudarev SL, Derlet PM, Van Swygenhoven H. 2009. The non-degenerate core structure of a $\langle 111 \rangle$ screw dislocation in bcc transition metals modelled using Finnis-Sinclair potentials: the necessary and sufficient conditions. *Philos. Mag.* 89:3235–43
138. Itakura M, Kaburaki H, Yamaguchi M. 2012. First-principles study on the mobility of screw dislocations in bcc iron. *Acta Mater.* 60:3698–710
139. Moruzzi VL, Sommers CB. 1995. *Calculated Electronic Properties of Ordered Alloys*. Singapore: World Sci. 448 pp.
140. Nguyen-Manh D, Vitek V, Horsfield AP. 2007. Environmental dependence of bonding: a challenge for modelling of intermetallics and fusion materials. *Prog. Mater. Sci.* 52:255–98
141. Ruban AV, Abrikosov IA. 2008. Configurational thermodynamics of alloys from first principles: effective cluster interactions. *Rep. Prog. Phys.* 71:046501
142. Olsson P, Abrikosov IA, Vitos L, Wallenius J. 2003. Ab initio formation energies of Fe-Cr alloys. *J. Nucl. Mater.* 321:84–90

143. Olsson P, Abrikosov IA, Wallenius J. 2006. Electronic origin of the anomalous stability of Fe-rich bcc Fe-Cr alloys. *Phys. Rev. B* 73:104416
144. Olsson P, Domain C, Wallenius J. 2007. Ab initio study of Cr interactions with point defects in bcc Fe. *Phys. Rev. B* 75:014110
145. Klaver TPC, P. Olsson P, Finnis MW. 2007. Interstitials in Fe-Cr alloys studied by density functional theory. *Phys. Rev. B* 76:214110
146. Olsson P. 2009. Ab initio study of interstitial migration in Fe-Cr alloys. *J. Nucl. Mater.* 386–388:86–89
147. Terentyev D, Olsson P, Klaver TPC, Malerba L. 2008. On the migration and trapping of single self-interstitial atoms in dilute and concentrated Fe-Cr alloys: atomistic study and comparison with resistivity recovery experiments. *Comput. Mater. Sci.* 43:1183–92
148. Castin N, Bonny G, Terentyev D, Lavrentiev MY, Nguyen-Manh D. 2011. Modelling phase separation in Fe-Cr system using different atomistic kinetic Monte Carlo techniques. *J. Nucl. Mater.* 417:1086–89
149. Nguyen-Manh D, Lavrentiev MY, Muzyk M, Dudarev SL. 2012. First-principles models for phase stability and radiation defects in structural materials for future fusion power-plant applications. *J. Mater. Sci.* 47:7385–98
150. Pareige C, Roussel M, Novy S, Kuksenko V, Olsson P, et al. 2011. Kinetic study of phase transformation in a highly concentrated Fe-Cr alloy: Monte Carlo simulation versus experiments. *Acta Mater.* 59:2404–11
151. Dudarev SL, Peng LM, Whelan MJ. 1992. A treatment of RHEED from a rough surface of a crystal by an optical potential method. *Surf. Sci.* 279:380–94
152. Dudarev SL, Vvedensky DD, Whelan MJ. 1994. Statistical treatment of dynamical electron diffraction from growing surfaces. *Phys. Rev. B* 50:14525–38
153. Delczeg L, Johansson B, Vitos L. 2012. Ab initio description of monovacancies in paramagnetic austenitic Fe-Cr-Ni alloys. *Phys. Rev. B* 85:174101
154. Klaver TPC, Drautz R, Finnis MW. 2006. Magnetism and thermodynamics of defect-free Fe-Cr alloys. *Phys. Rev. B* 74:094435
155. Martinez E, Senninger O, Fu CC, Soisson F. 2012. Decomposition kinetics of Fe-Cr solid solutions during thermal aging. *Phys. Rev. B* 86:224109
156. Tucker JD. 2008. *Ab initio-based modeling of radiation effects in the Ni-Fe-Cr system*. PhD thesis, Univ. Wisconsin, Madison, WI
157. Klaver TPC, Hepburn DJ, Ackland GJ. 2012. Defect and solute properties in dilute Fe-Cr-Ni austenitic alloys from first principles. *Phys. Rev. B* 85:174111
158. Was GS, Wharry JP, Frisbie B, Wirth BD, Morgan D, et al. 2011. Assessment of radiation-induced segregation mechanisms in austenitic and ferritic-martensitic alloys. *J. Nucl. Mater.* 411:41–50
159. Olsson P, Klaver TPC, Domain C. 2010. Ab initio study of solute transition-metal interactions with point defects in bcc Fe. *Phys. Rev. B* 81:054102
160. Gorbatov OI, Korzhavyi PA, Ruban AV, Johansson B, Gornostyrev YN. 2011. Vacancy-solute interactions in ferromagnetic and paramagnetic bcc iron: ab initio calculations. *J. Nucl. Mater.* 419:248–55
161. Vincent E, Becquart CS, Domain C. 2006. Solute interaction with point defects in a Fe during thermal ageing: a combined ab initio and atomic kinetic Monte Carlo approach. *J. Nucl. Mater.* 351:88–99
162. Hackett MJ, Najafabadi R, Was GS. 2009. Modeling solute-vacancy trapping at oversized solutes and its effect on radiation-induced segregation in Fe-Cr-Ni alloys. *J. Nucl. Mater.* 389:279–87
163. Becquart CS, Domain C. 2012. Solute–point defect interactions in bcc systems: focus on first principles modelling in W and RPV steels. *Curr. Opin. Solid State Mater. Sci.* 16:115–25
164. Först CJ, Slycke J, Van Vliet KJ, Yip S. 2006. Point defect concentrations in metastable Fe-C alloys. *Phys. Rev. Lett.* 96:175501
165. Becquart CS, Domain C, Foct J. 2005. Ab initio calculations of some atomic and point defect interactions involving C and N in Fe. *Philos. Mag.* 85:533–40
166. Domain C. 2006. Ab initio modelling of defect properties with substitutional and interstitials elements in steels and Zr alloys. *J. Nucl. Mater.* 351:1–19
167. Fu CC, Meslin E, Barbu A, Willaime F, Oison V. 2008. Effect of C on vacancy migration in α-iron. *Solid State Phenom.* 139:157–64

168. Ohnuma T, Soneda N, Iwasawa M. 2009. First-principles calculations of vacancy-solute element interactions in body-centered cubic iron. *Acta Mater.* 57:5947–55
169. Nguyen-Manh D. 2009. Ab-initio modelling of point defect–impurity interaction in tungsten and other bcc transition metals. *Adv. Mater. Res.* 59:253–56
170. Liu YL, Zhou HB, Zhang Y, Lu GH, Luo GN. 2011. Interaction of C with vacancy in W: a first–principles study. *Comput. Mater. Sci.* 50:3213–17
171. Terentyev D, Bonny G, Bakaev A, Van Neck D. 2012. On the thermal stability of vacancy-carbon complexes in alpha iron. *J. Phys. Condens. Matter* 24:385401
172. Jourdan T, Fu CC, Joly L, Bocquet JL, Caturla MJ, Willaime F. 2011. Direct simulation of resistivity recovery experiments in carbon-doped α-iron. *Phys. Scr.* T145:014049
173. Terentyev D, Olsson P, Klaver TPC, Malerba L. 2008. On the migration and trapping of single self-interstitial atoms in dilute and concentrated Fe-Cr alloys: atomistic study and comparison with resistivity recovery experiments. *Comput. Mater. Sci.* 43:1183–92
174. Ortiz CJ, Caturla MJ, Fu CC, Willaime F. 2009. Impurity effects on He diffusion in α-Fe. *J. Nucl. Mater.* 386–388:33–35
175. Boutard J-L, Dudarev SL, Rieth M. 2011. Modelling structural and plasma facing materials for fusion power plants: recent advances and outstanding issues in the EURATOM fusion materials programme. *J. Nucl. Mater.* 417:1042–49
176. Fu CC, Willaime F. 2005. Ab initio study of helium in α-Fe: dissolution, migration, and clustering with vacancies. *Phys. Rev. B* 72:064117
177. Becquart CS, Domain C. 2006. Migration energy of He in W revisited by ab initio calculations. *Phys. Rev. Lett.* 97:196402
178. Seletskaia T, Osetsky Y, Stoller RE, Stocks GM. 2005. Magnetic interactions influence the properties of helium defects in iron. *Phys. Rev. Lett.* 94:046403
179. Willaime F, Fu CC. 2006. First principles calculations of helium solution energies in bcc transition metals. *Mater. Res. Soc. Proc.* 981:0981-JJ05-04
180. Fu CC, Willaime F. 2007. Interaction between helium and self-defects in α-iron from first principles. *J. Nucl. Mater.* 367–370:244–50
181. Seletskaia T, Osetsky Y, Stoller RE, Stocks GM. 2008. First-principles theory of the energetics of He defects in bcc transition metals. *Phys. Rev. B* 78:134103
182. Zhang L, Zhang Y, Lu GH. 2013. Structure and stability of He and He-vacancy clusters at a Σ5(310)/[001] grain boundary in bcc Fe from first principles. *J. Phys. Condens. Matter*. 25:095001
183. Zu XT, Yang L, Gao F, Peng SM, Heinisch HL, et al. 2009. Properties of helium defects in bcc and fcc metals investigated with density functional theory. *Phys. Rev. B* 80:054104
184. Dudarev SL, Bullough R, Derlet PM. 2008. Effect of the α-γ phase transition on the stability of dislocation loops in bcc iron. *Phys. Rev. Lett.* 100:135503
185. Zhou HB, Jin S, Shu XL, Zhang Y, Lu GH, Liu F. 2011. Stress tensor: a quantitative indicator of effective volume and stability of helium in metals. *EPL* 96:66001
186. Lucas G, Schäublin R. 2008. Helium effects on displacement cascades in α-iron. *J. Phys. Condens. Matter* 20:415206
187. Gerasimenko VI, Mikhailovskii IM, Neklyudov IM, Parkhomenko AA, Velikodnaya OA. 1998. Changes in the fine structure of grain boundaries, induced by the absorption of helium, and helium embrittlement. *Tech. Phys.* 43:803–8
188. Hickel T, Grabowski B, Körmann F, Neugebauer J. 2012. Advancing density functional theory to finite temperatures: methods and applications in steel design. *J. Phys. Condens. Matter* 24:053202; doi: 10.1088/0953-8984/24/5/053202
189. Lavrentiev MY, Nguyen-Manh D, Dudarev SL. 2010. Magnetic cluster expansion model for bcc-fcc transitions in Fe and Fe-Cr alloys. *Phys. Rev. B* 81:184202
190. Lavrentiev MY, Dudarev SL, Nguyen-Manh D. 2011. Magnetic cluster expansion model for high-temperature magnetic properties of iron and iron-chromium alloys. *J. Appl. Phys.* 109:07E123
191. Lavrentiev MY, Soulairol R, Fu CC, Nguyen-Manh D, Dudarev SL. 2011. Noncollinear magnetism at interfaces in iron-chromium alloys: the ground states and finite-temperature configurations. *Phys. Rev. B* 84:144203

192. Derlet PM. 2012. Landau-Heisenberg Hamiltonian model for FeRh. *Phys. Rev. B* 85:174431
193. Gordon PA, Neeraj T, Mendelev MI. 2011. Screw dislocation mobility in bcc metals: a refined potential description for α-Fe. *Philos. Mag.* 91:3931–45
194. Ma PW, Woo CH, Dudarev SL. 2008. Large-scale simulation of the spin-lattice dynamics in ferromagnetic iron. *Phys. Rev. B* 78:024434
195. Ma PW, Woo CH. 2009. Parallel algorithm for spin and spin-lattice dynamics simulations. *Phys. Rev. E* 79:046703
196. Ma PW, Dudarev SL, Semenov AA, Woo CH. 2010. Temperature for a dynamic spin ensemble. *Phys. Rev. E* 82:031111
197. Ma PW, Dudarev SL. 2012. Longitudinal magnetic fluctuations in Langevin spin dynamics. *Phys. Rev. B* 86:054416
198. Yao Z, Jenkins ML, Hernández-Mayoral M, Kirk MA. 2010. The temperature dependence of heavy-ion damage in iron: a microstructural transition at elevated temperatures. *Philos. Mag.* 90:4623–34
199. Duffy DM, Rutherford AM. 2009. Including electronic effects in damage cascade simulations. *J. Nucl. Mater.* 386–388:19–21
200. Ma PW, Dudarev SL, Woo CH. 2012. Spin-lattice-electron dynamics simulations of magnetic materials. *Phys. Rev. B* 85:184301; doi: 10.1103/PhysRevB.85.184301
201. Dudarev SL, Peng LM, Whelan MJ. 1993. Correlations in space and time and dynamical diffraction of high-energy electrons by crystals. *Phys. Rev. B* 48:13408–29
202. Peng LM, Dudarev SL, Whelan MJ. 2011. *High-Energy Electron Diffraction and Microscopy*. Oxford, UK: Oxford Univ. Press. 535 pp.
203. Race CP, Mason DR, Sutton AP. 2012. A new directional model for the electronic frictional forces in molecular dynamics simulations of radiation damage in metals. *J. Nucl. Mater.* 425:33–40
204. Correa AA, Kohanoff J, Artacho E, Sánchez-Portal D, Caro A. 2012. Nonadiabatic forces in ion-solid interactions: the initial stages of radiation damage. *Phys. Rev. Lett.* 108:213201. Erratum. 2012. *Phys. Rev. Lett.* 109:069901(E)
205. Zeb MA, Kohanoff J, Sánchez-Portal D, Arnau A, Juaristi JI, Artacho E. 2012. Electronic stopping power in gold: the role of *d* electrons and the H/He anomaly. *Phys. Rev. Lett.* 108:225504
206. Nazarov R, Hickel T, Neugebauer J. 2012. Vacancy formation energies in fcc metals: influence of exchange-correlation functionals and correction schemes. *Phys. Rev. B* 85:144118

Annual Review of
Materials Research

Volume 43, 2013

Contents

Current Interest